

# Chemical and antibacterial effects of plasma activated water: correlation with gaseous and aqueous reactive oxygen and nitrogen species, plasma sources and air flow conditions

Z Machala<sup>1</sup>, B Tarabová<sup>1</sup>, D Sersenová, M Janda<sup>1</sup> and K Hensel<sup>1</sup>

Faculty of Mathematics, Physics and Informatics, Comenius University, Mlynska Dolina, 84248 Bratislava, Slovakia

E-mail: [machala@fmph.uniba.sk](mailto:machala@fmph.uniba.sk)

Received 13 July 2018, revised 3 October 2018

Accepted for publication 12 October 2018

Published 9 November 2018



## Abstract

When cold atmospheric plasma comes into contact with water and biological media, antimicrobial or antitumor effects are induced, representing great potential for applications in biomedicine and agriculture. The need to control and tune the chemical composition and biomedical effects of plasma activated water/media (PAW/PAM) is emerging. By comparing two nonthermal air plasma sources, streamer corona and transient spark, interacting with water in open and closed reactors, and by enhancing the plasma–liquid interaction by water electrospray through these discharges, we demonstrate that the plasma gaseous products strongly depend on the discharge regime, its deposited power and gas flow conditions. The streamer corona strongly leads to the formation of ozone and hydrogen peroxide, while the more energetic transient spark leads to nitrogen oxides and hydrogen peroxide. The gaseous products then determine the chemical properties of the PAW and the dominant aqueous reactive oxygen and nitrogen species (RONS). The production of hydrogen peroxide depends on water evaporation and hydroxyl radical formation, which is determined by the discharge power. A transient spark produces higher concentrations of gaseous and aqueous RONS and induces stronger antibacterial effects than a streamer corona; however, the RONS production rates per joule of deposited energy are comparable for both studied discharge regimes. The net production rate per joule of gaseous nitrogen oxides strongly correlates with that of aqueous nitrites and nitrates. The antibacterial effects of the PAW tested on *Escherichia coli* bacteria are determined by the aqueous RONS: in the lower power streamer corona, this is ascertained mainly by the dissolved ozone and hydrogen peroxide, and in the higher power transient spark, by the combination of hydrogen peroxide, nitrite and acidic pH, while in the transient spark in the closed reactor it is determined by the acidified nitrites present.

Keywords: non-thermal air plasma, plasma activated water, reactive oxygen and nitrogen species (RONS), antibacterial effects

(Some figures may appear in colour only in the online journal)

---

<sup>1</sup> Author to whom any correspondence should be addressed.

## List of abbreviations

CFU	Colony forming unit
DBD	Dielectric barrier discharge
DC	Direct current
ES	Electrospray
FTIR	Fourier transform infrared spectroscopy
HV	High voltage
PAM	Plasma activated medium
PAW	Plasma activated water
RNS	Reactive nitrogen species
ROS	Reactive oxygen species
RONs	Reactive oxygen and nitrogen species
SC	Streamer corona
SC-ES	Streamer corona with electrospray
TS	Transient spark
TS-ES	Transient spark with electrospray

## 1. Introduction

Water and aqueous solutions (media) treated/activated by cold atmospheric pressure plasmas—so called plasma activated water (PAW) or plasma activated media (PAM)—are currently of great interest for multiple applications in biomedicine and agriculture [1, 2], mainly due to their antimicrobial and antitumor properties. Nonthermal (nonequilibrium, cold) atmospheric pressure plasmas generated in air or N<sub>2</sub>–O<sub>2</sub> mixtures, or noble gases blown into the ambient air atmosphere, produce various radicals and reactive molecules commonly called reactive oxygen and nitrogen species (RONS). They are e.g. hydroxyl radicals  $\bullet\text{OH}$ , hydrogen peroxide H<sub>2</sub>O<sub>2</sub>, nitrogen oxides N<sub>2</sub>O, NO, NO<sub>2</sub>, ozone O<sub>3</sub>, and superoxide O<sub>2</sub><sup>•-</sup>. In plasma discharges interacting with water, water evaporation supports the formation of OH radicals and H<sub>2</sub>O<sub>2</sub> in the gas. The primary gaseous RONS are transported through the plasma–liquid interface and induce the formation of secondary aqueous RONS in the water, such as  $\bullet\text{OH}$ , H<sub>2</sub>O<sub>2</sub>, nitrites/nitrates NO<sub>2</sub><sup>-</sup>/NO<sub>3</sub><sup>-</sup>, peroxyxynitrites/peroxyxynitrous acid ONOO<sup>-</sup>/ONOOH, peroxyxynitrates/peroxyxynitric acid O<sub>2</sub>NOO<sup>-</sup>/O<sub>2</sub>NOOH, superoxid/perhydroxyl radical O<sub>2</sub><sup>•-</sup>/HO<sub>2</sub><sup>•</sup>, or O<sub>3</sub>. In biomedical plasma applications, such as dentistry, wound healing or tumor treatment, the tissue is usually covered by a thin layer of an aqueous biological liquid. The RONS generated by the plasma activate and interact with the liquid layer before they reach the tissue. PAW and PAM, or cold plasmas mediated through aqueous layers, induce antimicrobial or therapeutic effects applicable in medicine, agriculture and food processing [3–21]. These effects occur thanks to the emerging role of plasma generated RONS, sometimes combined with the effects of other plasma agents (e.g. electric field, electrons and ions, UV radiation), and the RONS chemistry induced in aqueous media.

A recent roadmap on plasma–liquid interactions reports on the key challenges and areas for further studies in order to obtain a deeper understanding of the chemical and physical processes occurring when plasma interacts with a liquid surface, particularly with water [1]. A number of studies deal

with the aqueous RONS diagnostics in the PAW or PAM and attempt to identify RONS that are responsible for the antimicrobial or other biomedical/decontamination effects [6, 9, 10, 12, 14, 16, 17, 19–38]. There are only a few research papers that extensively investigated the ambient air plasma chemistry and RONS, their transport through the plasma–liquid interface into water and induced aqueous RONS, and the biomedical effects of the plasma activated water/media (PAW/PAM) to provide an effective control of plasma–liquid interactions for biomedical applications. For example, the Ar radio frequency plasma jet (KINPen), with various shielding gas curtains, was extensively investigated and applied to multiple biomedical uses, including clinical tests [6]. Several research groups varied a shielding gas composition around the plasma jets to control the production of RONS with the possibility of varying ratios of O<sub>2</sub>/N<sub>2</sub> [18, 23, 32]. The importance of effective control of the gaseous plasma environment processes was demonstrated by analyzing biological responses and RONS generation induced by cold plasmas [23, 32, 39]. Girard *et al* also applied O<sub>2</sub>/N<sub>2</sub> shielding to the He plasma jet and analyzed plasma emission in the vicinity of the liquid, and aqueous RONS in phosphate buffer saline (PBS), to control plasma–air interactions and better understand a complex interplay between plasma jet ionization waves and liquids [40].

Another group of studies, including the present one, deal with nonequilibrium plasmas operated directly in air and their interactions with aqueous liquids. Atmospheric pressure plasma jets cannot be easily run in air mixtures (without noble gases); nevertheless, air plasma discharges also enable applicability to liquids or biomedical targets with high efficiency, since air components are the optimal precursors of RONS. Several authors reported different gas-phase and related aqueous RONS chemistries with low and high power nonequilibrium air plasma discharges. Pavlovich *et al* operated surface microdischarge (surface DBD) and reported that low power resulted dominantly in O<sub>3</sub> production that consequently dissolved in water, and this aqueous O<sub>3</sub> was strongly antimicrobial, while high power resulted dominantly in NO<sub>x</sub> that were also antibacterial [12]. Nani *et al* compared positive and negative coronas and DBD operated in air above water contaminated with metolachlor pesticide and identified the higher efficiency in the negative corona discharge that produced the highest  $\bullet\text{OH}$  and H<sub>2</sub>O<sub>2</sub> concentrations [36]. Lu *et al* compared AC-driven (25 kHz) spark and glow discharges with a water electrode and found that the lower power spark lead dominantly to H<sub>2</sub>O<sub>2</sub> and NO<sub>3</sub><sup>-</sup>, while higher power glow discharge dominantly produced reactive nitrogen species (RNS) (NO<sub>2</sub><sup>-</sup> and NO<sub>3</sub><sup>-</sup>) in PAW. H<sub>2</sub>O<sub>2</sub> production was even enhanced by increasing water vapor pressure in the discharge [17]. In a similar way, Modic *et al* compared antibacterial effects of air DBD with low power (8 W) leading dominantly to reactive oxygen species (ROS) and high power (35 W) dominated by RNS on biofilms exposed directly to the plasma [19].

In order to better understand and control RONS production in air plasma, their transport into water and related biomedical effects, in this paper, we compare two different cold air plasma sources (discharge regimes): a lower power streamer corona and a higher power transient spark. We demonstrate

different properties and antibacterial effects of the PAWs generated in these discharges due to different gas-phase chemistries controlling the production of active plasma species, such as  $O_3$ ,  $H_2O_2$ , NO and  $NO_2$  [41]. It has been reported by several research groups that reactors that utilize thin liquid films, foams, or fine liquid droplets are typically more efficient than other configurations for chemical oxidation and formation of  $H_2O_2$  [8, 42–45]. The main reason is the increased surface area of the plasma–liquid interface that promotes water evaporation and the transfer of species from the plasma into the water. Droplet size or thin film thickness determines the transport phenomena of various RONS that have various Henry’s law solubility coefficients [46, 47]. This is our key motivation to prepare PAW by applying water electrospray to inject fine aerosol droplets directly through the active plasma zone, which results in a very efficient transfer of gaseous RONS into water. In addition, we demonstrate that besides the discharge regime and power, and plasma–liquid interface area, the gas flow conditions through the plasma reactor, especially the reactor volume and gas flow rate strongly influence the gaseous RONS formation rates and consequently their transport into water and thus the PAW properties.

In this study, we focus on nonbuffered water which has great potential as an antimicrobial agent in disinfection, wound healing or dentistry. For example, we previously demonstrated strong inactivation of biofilms by DC corona discharges with water electrospray [15]. The buffering capacity of aqueous solutions fixing certain pH values strongly influence the aqueous RONS concentrations and mutual reactions, and consequently the PAW biorelevant effects [10, 24]. We find correlations of the discharge regime and gas flow conditions with gaseous, and consequently with aqueous RONS, transported into and formed in the water, and attempt to relate them to the antibacterial effects of PAW tested on *Escherichia coli* (*E. coli*) bacteria. To the best of our knowledge, this is one of the very few studies that provide insight into these complex correlations of air plasma gaseous and aqueous RONS chemistry with antibacterial effects in one paper. The controlled and selective generation of RONS using air plasmas with water will facilitate targeted applications of cold plasmas and PAW to various fields including disinfection and antimicrobial applications, food processing, agriculture, and even cancer therapies, where the roles of different key reactive species on cancer cell biochemistry is particularly delicate [5, 17].

## 2. Experimental setups and methods

### 2.1. Streamer corona and transient spark air plasma discharges

DC-driven streamer corona and transient spark discharges in positive polarity were generated in point-to-plane configuration in ambient air at atmospheric pressure.

A streamer corona (SC) is typical for small current pulses of streamers ( $\sim 10$  mA) with a 5–20 kHz repetition rate, and generates cold nonequilibrium air plasma ( $\sim 300$  K). With increasing voltage, the streamers establish a conductive channel that gradually leads to a spark breakdown with

excessive current pulse. However, this current pulse is limited by the ballast resistor  $R$  that drops the voltage and by the small capacity between the electrodes (in the order of 10 pF). Thus, when the spark forms, it is only transient since the discharged energy is small (0.1–1 mJ). This transient spark (TS) is a repetitive (0.5–10 kHz) streamer-to-spark transition discharge, with each spark pulse ( $\sim 1$ –30 A) preceded by one or a sequence of streamer pulses. Thanks to the very short pulse duration ( $\sim 10$ –100 ns), the TS plasma remains nonequilibrium at relatively low gas temperature ( $\sim 350$ –600 K) although shortly after the spark pulse the temperature temporarily exceeds 1000 K inside the plasma channel for a very short time ( $\sim 10$ –100 ns). The self-pulsing repetitive transient spark discharge has been studied and described in detail in our previous work [48–50]. The positive streamer corona regime used here has been described in more detail, for example in [15].

We used a high voltage (HV) hollow needle anode opposite the metallic (stainless steel) grounded mesh cathode. The inter-electrode spacing between the needle and the mesh was kept at 10 mm. A positive HV was applied from the power supply (Technix SR20-R-1200) through the ballast resistor  $R$  (20 M $\Omega$  for SC or 10 M $\Omega$  for TS). The discharge voltage was measured by the HV probe (Tektronix P6015A) and the discharge current was measured as a voltage drop across 50 or 1.2  $\Omega$  resistors for SC and TS, respectively. The electrical parameters were processed and recorded during the experiments by a 200 MHz oscilloscope (Tektronix TDS 2024C). Typical current and voltage waveforms and other discharge characteristics of SC and TS discharge with water electrospray or water cathode, were documented in detail in our previous publications [8, 10, 14, 15, 51, 52]. Both TS and SC, as two different discharge regimes with different induced gaseous and aqueous chemistries, can be operated in the same versatile setup with the same HV power supply, which represents an advantage for practical applications. We only changed the ballast and current-monitoring resistors to switch between TS and SC.

### 2.2. Electrospray water activation

A simple way to efficiently activate water by cold air plasma discharges is to generate the plasma discharge between the HV (stressed) electrode and the water surface, with the water surface acting as the other discharge electrode (typically grounded), in air atmosphere [14, 51, 53]. More efficient water activation can be achieved by a combination of water electrospray with the discharge. The water electrospray system (ES) enables the water to flow directly through the HV needle electrode into the active discharge region, where it is sprayed in micrometric droplets (figure 1). The interaction of plasma with water droplets allows for the very efficient mass transfer of plasma generated active species through the plasma–liquid interface into water [8, 10, 52]. In this case, the HV hollow needle electrode allowed for the injection of water with the various flow rates in the range 0.01–1 ml min $^{-1}$  by the syringe pump (New Era Pump Systems NE-300), directly through the active discharge zone. Due to the applied HV on the needle electrode, the effect of water electrospray in fine micrometric

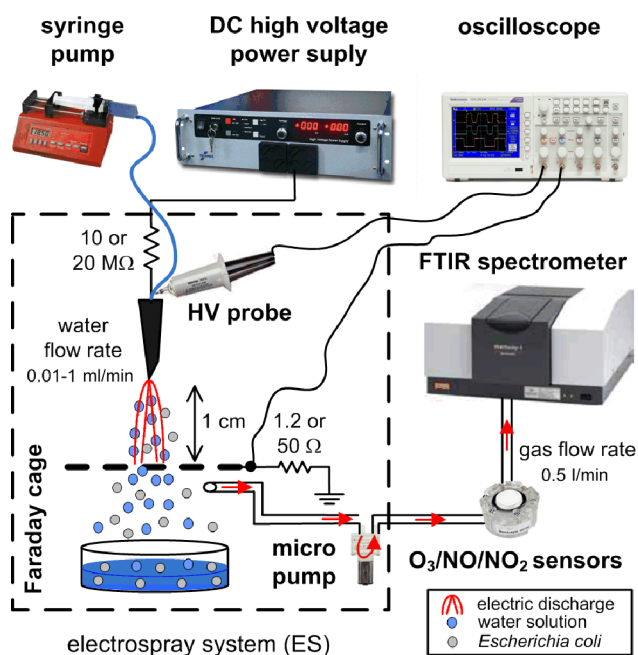


**Figure 1.** Experimental setup for water electro spray through streamer corona or transient spark discharge.

size droplets occurred [15, 52]. The needle nozzle with a special cut facilitated better contact of the water droplets with the discharge. In the following text, a combination of SC and TS discharge with water electro spray will be designated as SC-ES and TS-ES.

### 2.3. Open and closed reactor

All experiments presented in this study were performed in ambient air without or with a water electro spray system. In most of our previous studies [8, 10, 14, 15, 37] we ran both SC and TS discharges in the *open reactor*, in ambient atmosphere without any reactor walls. Such a setup enables a fast exchange of gases: diffusion and hydrodynamic expansion of plasma created gaseous species out of the discharge channel and fast refreshment of the ambient air into the discharge space, with associated gas cooling.

We also operated the same plasma discharges in a *closed reactor* (50 ml volume) with a defined air flow rate. This air flow rate determines the gas mixing and accumulation of species produced by the plasma. We varied gas flow rates through the closed reactor from low ( $0.5 \text{ l min}^{-1}$ ) to high ( $1.71 \text{ l min}^{-1}$ ). Later we will show that this dramatically changes the plasma chemistry in the gas and consequently in the aqueous phase.

### 2.4. Diagnostics of gas-phase plasma products

The experiments focussing on the diagnostics of the gas-phase discharge products were carried out in the open or closed 50 ml reactor in ambient air. The analyzed gas was pumped through a gas tube (PTFE, 6 mm o.d., 4 mm i.d.) placed directly below the grounded mesh electrode by the air pump with a constant flow rate of  $0.5 \text{ l min}^{-1}$ .

NO and NO<sub>2</sub> concentrations were measured online by electrochemical gas sensors (Membrapor NO<sub>2</sub>/S-1000 and NO/SF-1000 with resolution 5 ppm, range 0–1000 ppm) or a gas analyzer (Kane KM9106 Quintox) to detect 0–1000 ppm NO and NO<sub>2</sub> electrochemically with 3% accuracy in ambient air measurements without water. In addition, a Fourier transform infrared (FTIR) absorption spectrophotometer (Shimadzu IRAffinity-1S) was used for the detection of gaseous nitrogen oxides NO, NO<sub>2</sub> and N<sub>2</sub>O; nitric and nitrous acids HNO<sub>3</sub>, HNO<sub>2</sub>, and ozone O<sub>3</sub> with the resolution  $1 \text{ cm}^{-1}$  inside a 10 cm long gas cell. The following vibrational bands were used as diagnostics for the presence of reactive species: NO at  $1900 \text{ cm}^{-1}$ ; NO<sub>2</sub> at  $1627$  and  $2916 \text{ cm}^{-1}$ ; N<sub>2</sub>O at  $2235 \text{ cm}^{-1}$ , HNO<sub>3</sub> at  $1325$  and  $1718 \text{ cm}^{-1}$ ; HNO<sub>2</sub> at  $1260 \text{ cm}^{-1}$ . The absolute concentrations of NO and NO<sub>2</sub> were estimated from the FTIR bands based on calibration with commercial gas mixtures (1000 ppm NO<sub>2</sub> in air and 2000 ppm NO in N<sub>2</sub>, Linde) in various dilutions and parallel measurements with the gas sensors.

Ozone concentrations were measured online, based on the UV absorption, by a homemade ozone analyzer using a 253.8 nm mercury lamp and the compact fiber optic spectrometer (OceanOptics SD2000), employing the Lambert–Beer law with the absorption cross section  $1.14 \times 10^{-21} \text{ m}^2$  [54] in a 12.5 cm gas cell. An FTIR absorption band of O<sub>3</sub> at  $1055 \text{ cm}^{-1}$  was also used for higher concentrations.

### 2.5. Diagnostics of aqueous RONS in PAW

We used a dilute NaH<sub>2</sub>PO<sub>4</sub> water solution (pH 5.5,  $\sigma = 600 \mu\text{S cm}^{-1}$ ) that mimics tap water in conductivity and has no buffering capacity, to be able to compare with our previous results obtained with this water solution [10, 37]. The detection of RONS in the PAW is challenging due to the chemical instability of the detected RONS and possible cross-reactivities of the analytical methods used. We adapted established colorimetric methods for special PAW conditions, such as colorimetric detection of H<sub>2</sub>O<sub>2</sub> using TiOSO<sub>4</sub> reagent, and O<sub>3</sub> by indigo blue assay [10, 37] measured by a UV/VIS absorption spectrophotometer (UV-1800 Shimadzu).

Measurement of hydrogen peroxide was performed by the titanium oxysulfate assay based on the reaction of H<sub>2</sub>O<sub>2</sub> with the titanium (IV) ions under acidic conditions. The yellow-colored product of perititanic acid H<sub>2</sub>TiO<sub>4</sub> is formed with the absorption maximum at 407 nm [55]. The concentration of H<sub>2</sub>O<sub>2</sub> is proportional to the absorbance according to Lambert–Beer's law (molar extinction coefficient  $\epsilon = 6.89 \times 10^2 \text{ l mol}^{-1} \text{ cm}^{-1}$ ). Because of the possible H<sub>2</sub>O<sub>2</sub> decomposition by NO<sub>2</sub><sup>-</sup> under acidic conditions, sodium azide (NaN<sub>3</sub>, 60 mM) was added to the sample prior to mixing with the titanium oxysulfate reagent [24]. Sodium azide immediately reduces nitrites into molecular nitrogen and preserves the H<sub>2</sub>O<sub>2</sub> concentration intact.

Aqueous nitrites NO<sub>2</sub><sup>-</sup> and nitrates NO<sub>3</sub><sup>-</sup> were measured by Griess reagents. This colorimetric method is based on the reaction of NO<sub>2</sub><sup>-</sup> with the Griess reagents under acidic conditions, which convert into a deep purple azo compound with the absorption maximum at 540 nm. We used a Cayman Chemicals Nitrate/Nitrite Colorimetric Assay Kit #780001

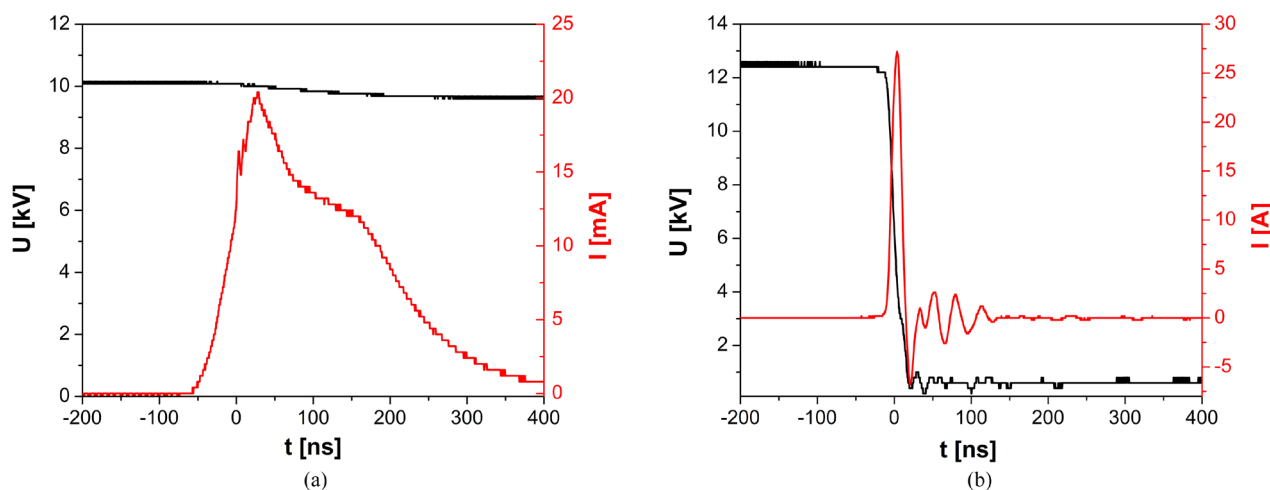


**Figure 2.** The typical voltage and current pulse waveforms of SC (a) and TS (b) with water electro spray.

that contained already-prepared ready-to-use Griess reagents. Nitrates were converted into nitrites using the nitrate reductase enzyme and subsequently analyzed the same way as nitrites.

The detection of the dissolved ozone was performed by the indigo blue assay. It is a simple and quantitative colorimetric standardized method for ozone detection in water and waste water [56]. In acidic conditions  $O_3$  rapidly decolorizes the indigo potassium trisulfonate dye and the colourless product isatin is formed by the bleaching process. The decrease of the absorbance at 600 nm ( $\epsilon = 2.38 \times 10^4 \text{ M}^{-1} \text{ cm}^{-1}$ ) is linear with the increasing concentration of dissolved  $O_3$ . However, we must note that this method may not be specific enough for  $O_3$ . We previously showed that it may give false signals, especially due to OH radicals or other RONS in the PAW, and is absolutely not suitable for the  $O_3$  analysis in transient spark PAW, where no  $O_3(\text{aq})$  was detected by other methods (phenol as the chemical probe and its specific degradation products) [37]. Therefore, we only applied the indigo blue method for  $O_3(\text{aq})$  analysis in the streamer corona PAW.

### 2.6. Diagnostics of antibacterial effects

Antibacterial effects were tested on gram-negative bacteria *E. coli* (ATCC 25922) suspended in water in planktonic form with initial populations from  $10^6$  to  $10^7$  colony forming units per ml (CFU  $\text{ml}^{-1}$ ). The microbial cultivation was carried out in a sterile environment. Starting from an overnight bacterial culture in a shaker with sterile liquid nutrient (Lauria-Bertani broth, Biolab), bacteria were diluted in water to obtain the desired concentrations. The plasma experiments with bacteria suspensions were performed with TS and SC, operating in ambient atmospheric air with water electro spray, in the open and closed reactors, and repeated three to ten times. The number of bacteria cells in the suspension was evaluated immediately after plasma treatment by counting colony forming units (CFUs) cultivated on agar plates (Lauria Bertani agar, Biolab) over 16–18 h at 37 °C. Several ten-fold dilution series were used to achieve the optimum number of CFUs grown on agar plates, especially for controls and low inactivation rates. For high inactivation rates of plasma treated water solution

(~6 logs reduction), no dilutions were needed. Usually, four to six agar plates from each sample were taken for statistical evaluation. The viability of bacteria was determined as the ratio of the population of surviving bacteria in plasma treated samples to the total population in reference samples. The lowest detection limit of 2 CFU  $\text{ml}^{-1}$  was calculated.

## 3. Results and discussion

### 3.1. Streamer corona and transient spark discharge parameters

Both discharges used in this study are driven by DC HV but are self-pulsing. Their typical characteristics are shown below.

- *Streamer corona (SC)*: mean power 0.2–0.4 W, pulse frequency typically ~10 kHz, operated with water electro spray flow rates of 0.01–0.5  $\text{ml min}^{-1}$  and variable activation time to collect enough water volume for further aqueous RONS analyses (typically 1–2 ml). The typical voltage and current pulse waveforms of SC-ES are depicted in figure 2(a).
- *Transient spark (TS)*: mean power 1.5–2.3 W, typical pulse frequency ~1 kHz, in some cases we increased the frequency up to 4 kHz (with the corresponding mean power up to 8 W), typical pulse duration ~25 ns. TS was operated with water electro spray flow rates 0.5–1  $\text{ml min}^{-1}$  and variable activation times to collect enough water volume for further aqueous RONS analyses (typically 1–2 ml). The typical voltage and current pulse waveforms of TS-ES are depicted in figure 2(b).

### 3.2. Gas-phase diagnostics and chemistry in ambient air without water

Electrons in SC and during the initial streamer phase of the TS discharge have enough energy to ionize and dissociate the dominant air molecules  $N_2$  and  $O_2$ . The direct electron impact dissociation of  $N_2$  is much slower than that of  $O_2$  and so the major intermediate product is the atomic oxygen  $\bullet O$ . The

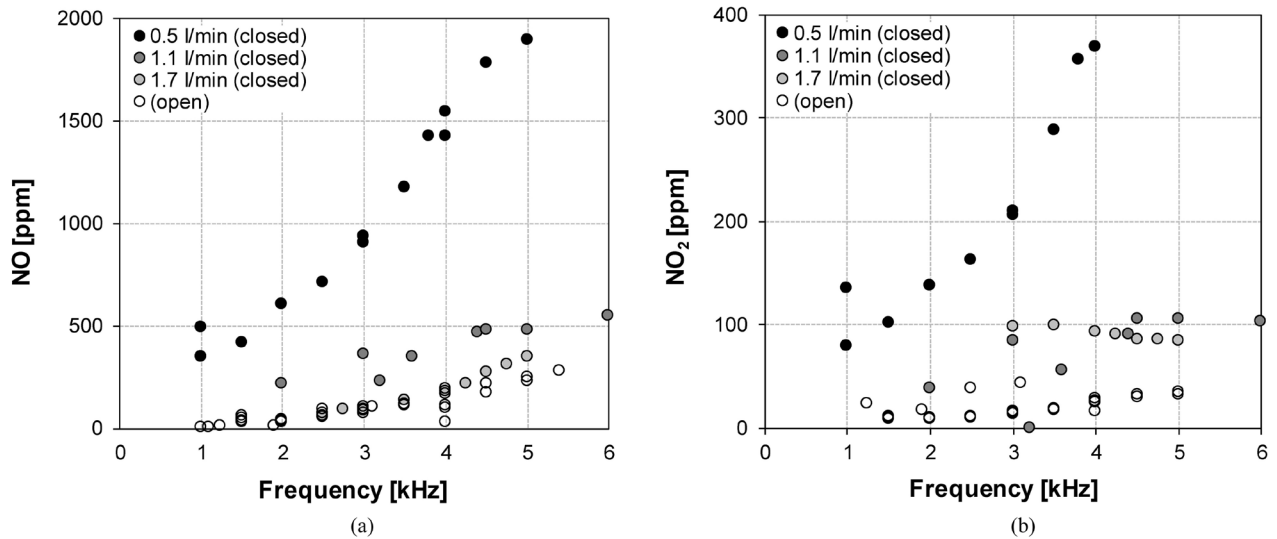
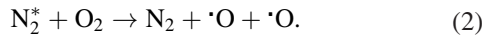


**Figure 3.** Gaseous NO (a) and NO<sub>2</sub> (b) formation by TS in ambient air (without water)—open versus closed reactor, various air flow rates through the reactor.

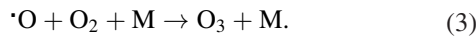
electron collision with N<sub>2</sub> leads preferentially to the formation of various excited N<sub>2</sub><sup>\*</sup> molecules (equation (1)):



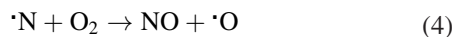
Fast quenching of the excited N<sub>2</sub><sup>\*</sup> molecules with molecular oxygen is the additional source of atomic oxygen (equation (2)) [57]:



At low gas temperature, ozone is generated from the accumulated  $\cdot O$  atoms via a relatively slow three-body reaction:

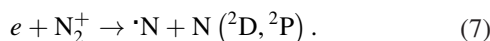
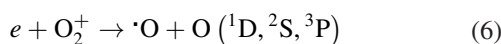


Formation of NO can proceed via the Zeldovich mechanism (equations (4) and (5)):



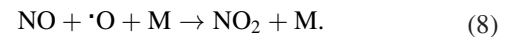
The limiting factor for the NO generation in SC is the insufficient amount of  $\cdot N$  atoms (in equation (4)) and the low gas temperature (in equation (5)). As a result, O<sub>3</sub> is the major product of the SC in air.

In the TS spark phase, the increase of the gas temperature [48, 49] causes decomposition of O<sub>3</sub> and enhances NO formation via the Zeldovich mechanism. In addition, a high degree of ionization and atomization can accelerate this chain reaction. The production of atomic  $\cdot O$  and  $\cdot N$  can also be enhanced via the dissociative recombination of electrons with N<sub>2</sub><sup>+</sup> and O<sub>2</sub><sup>+</sup> ions (equations (6) and (7)) [41]:



These reactions enhance the NO<sub>x</sub> synthesis, especially due to  $\cdot N$  production.

The  $\cdot O$  production is also enhanced by equation (6) and it could lead to the post-discharge O<sub>3</sub> generation in colder gas away from the plasma channel. However, once there is enough NO, the  $\cdot O$  atoms can trigger oxidation of NO into NO<sub>2</sub> in a three-body reaction (equation (8)):



Furthermore, generated O<sub>3</sub> could be depleted by oxidizing NO to NO<sub>2</sub> (equation (9)):



Reactions (equations (8) and (9)) were also identified as dominant NO<sub>2</sub> production channels in the chemical kinetic modeling of an atmospheric plasma jet [58]. All these reactions above explain why NO and NO<sub>2</sub> are dominant products in the TS with negligible O<sub>3</sub> production, unlike in the SC where O<sub>3</sub> dominates over NO<sub>x</sub> formation.

Figure 3 shows gaseous NO and NO<sub>2</sub> concentrations generated in the ambient air TS (without water) as a function of the pulse frequency that is approximately proportional to the discharge power, for the open and closed reactor with various air flow rates. As one would expect, and in agreement with our previous results on NO<sub>x</sub> formation in the TS discharge [41], as well as other studies in plasma jets [59], the higher discharge frequency (i.e. power) results in higher NO and NO<sub>2</sub> formation. Concentrations of NO were in general much higher than those of NO<sub>2</sub>. This is because NO is the primary product of the Zeldovich mechanism (equations (4) and (5)), while NO<sub>2</sub> is formed by later NO oxidation with  $\cdot O$  or O<sub>3</sub> (equations (8) and (9)), which are much slower and cannot oxidize most of the formed NO, as there is not sufficient time between the TS discharge pulses (the typical frequency is ~1 kHz or more).

We can see a stark difference between NO<sub>x</sub> concentrations in the open and closed reactors in figure 3. The significant air flow rate effect is also evident: the slower the gas flow rate through the closed reactor, the higher the NO and NO<sub>2</sub> concentrations due to the longer accumulation of reactive species in the reactor volume. The lowest NO<sub>x</sub> concentrations were in

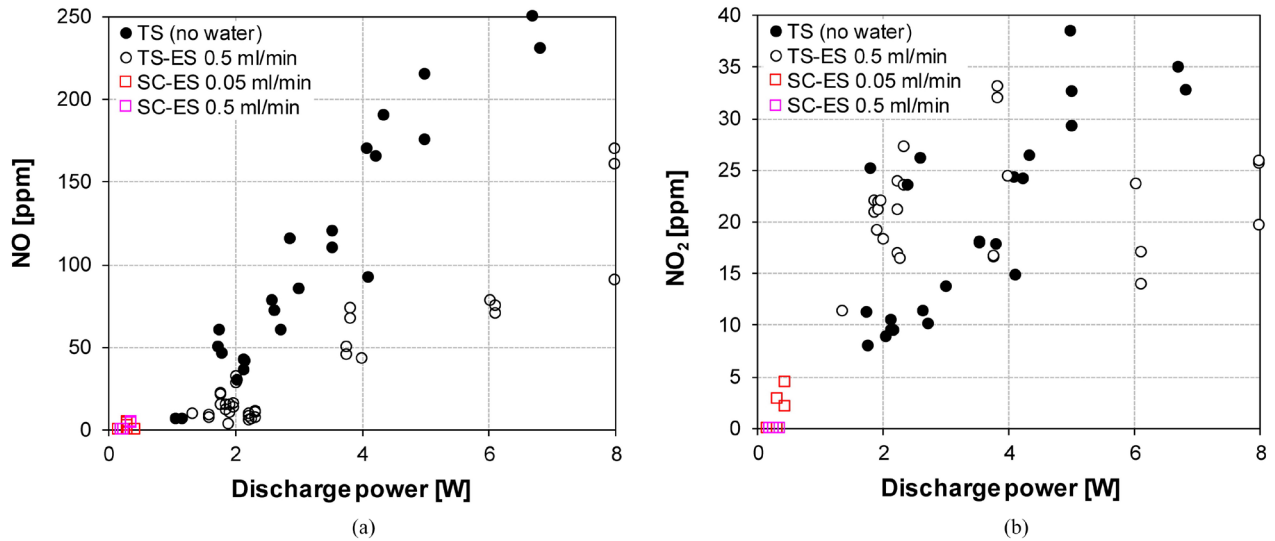
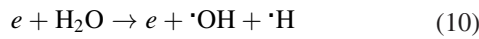


**Figure 4.** Gaseous NO (a) and NO<sub>2</sub> (b) formed by TS and SC in ambient air without and with water electro spray as a function of discharge power—open reactor, 0.5 l min<sup>-1</sup> air flow rate.

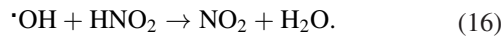
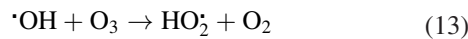
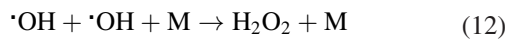
the open reactor where the fastest mixing with surrounding air and diffusion of species occurred. In addition, the sampled gas pumped from below the mesh electrode was diluted with the ambient air in the open reactor.

### 3.3. Gas-phase diagnostics and chemistry in ambient air with water electro spray

Water vapors in air can significantly influence the plasma induced gas-phase chemistry. The highly reactive hydroxyl (<sup>•</sup>OH) radical can be produced by several reactions (equations (10) and (11)) [60]:



<sup>•</sup>OH radicals can react with themselves and with all major plasma species observed in air resulting in further ROS such as H<sub>2</sub>O<sub>2</sub> and HO<sub>2</sub><sup>•</sup>, and RNS such as HNO<sub>2</sub> and HNO<sub>3</sub> (equations (12)–(16)):

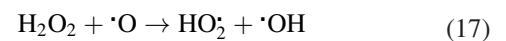


We can thus expect lower concentrations of NO, NO<sub>2</sub> and O<sub>3</sub> in the gas phase in humid air compared to in the dry air. When the discharges are operated with water electro spray, there is a strong water evaporation and humidification of the air, which should enhance the <sup>•</sup>OH formation and consequently the reactions (equations (10)–(16)). Moreover, the transport of NO, NO<sub>2</sub>, O<sub>3</sub>, and other species such as HNO<sub>2</sub> into the bulk water, i.e. their solvation driven by Henry's Law equilibria, should also decrease NO, NO<sub>2</sub> and O<sub>3</sub> concentrations in the gas

phase. The situation is in fact even more complicated because the discharge properties and NO<sub>x</sub>/O<sub>3</sub> generation efficiencies may also change due to the presence of the water, e.g. the gas temperature can be reduced due to the energy spent for water evaporation. In our previous study we have indeed determined lower gas temperature (as the N<sub>2</sub>(C) rotational temperature) in the TS-ES with respect to TS in ambient air without water [37].

The NO concentration generated by TS was found to be considerably lower in air humidified by the water electro spray (TS-ES) compared to the TS in ambient air without water, as shown in figure 4(a) as a function of the discharge power. The water electro spray through the plasma increases the interfacial surface of electro sprayed micrometric droplets and so presumably improves the gas–liquid transport of the gaseous NO<sub>x</sub> into the liquid resulting in NO<sub>x</sub> dissolution in the water. The lower NO in TS-ES is possibly also due to the discharge cooling by water evaporation and thus suppressed NO formation in the gas [37]. The NO<sub>x</sub> dissolution into the electro sprayed water microdroplets depleted NO<sub>x</sub> from the air. NO formation in SC-ES was considerably lower compared to TS-ES due to the much lower power.

Despite relatively scattered measured data points of NO<sub>2</sub> concentrations (figure 4(b)), it is clear that NO<sub>2</sub> formation in general increased with the discharge power in all systems and SC generated considerably lower NO<sub>2</sub> due to the lower discharge power. Interestingly TS-ES generated higher concentrations of NO<sub>2</sub> than TS without water, in agreement with our previous results [37], especially for low discharge powers. This effect can have several possible explanations. At low discharge power, some O<sub>3</sub> may be generated and may quickly oxidize NO to NO<sub>2</sub> by the reaction (equation (9)). In addition, due to the water vapor dissociation, peroxy radicals HO<sub>2</sub><sup>•</sup> are produced by several possible pathways, e.g. by the reaction with O<sub>3</sub> (equation (13)) or the following ones without O<sub>3</sub> (equations (17)–(19)):



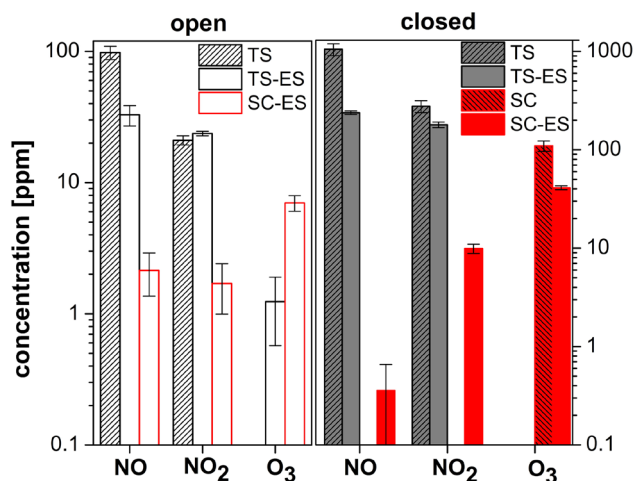
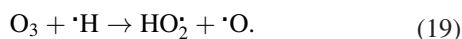
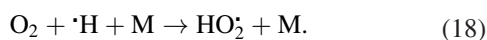
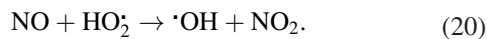


**Figure 5.** Gaseous NO, NO<sub>2</sub> and O<sub>3</sub> concentrations generated by TS and SC discharges, without and with water ES, in the open and closed (50 ml, 0.5 l min<sup>-1</sup> air flow) reactors. Logarithmic scale. Statistical mean values with standard error of the mean (SEM).



HO<sub>2</sub><sup>•</sup> can also oxidize NO to NO<sub>2</sub> and so enhance the NO<sub>2</sub> formation at the expense of NO and release <sup>•</sup>OH radicals (equation (20)).



Deciphering the respective roles of the above and other relevant reactions will require further research, including chemical kinetic modeling. Nevertheless, they can together enhance the NO to NO<sub>2</sub> conversion, especially at low discharge power, and explain the fact that TS-ES produced higher NO<sub>2</sub> than TS without water (unlike for the case of the NO production).

Seeing that the experimental data points are relatively scattered, it should be noted that once the water was electrospayed into relatively regularly repetitive and stable TS discharge, the TS pulses became less regular, and their frequency jittered. Therefore, the exact power measurement was more challenging with ES, and all the TS-ES data points presented in figure 4 should be perhaps presented with horizontal error bars as wide as ±0.5 W. Vertical error bars of the data points in figure 4 are determined by the accuracy of NO and NO<sub>2</sub> concentration measurements given by the electrochemical sensors and FTIR spectral analysis and should be at least ±5 ppm. This is especially important for NO<sub>2</sub> where concentrations were generally lower than NO.

It is demonstrative to compare the NO, NO<sub>2</sub> and gaseous O<sub>3</sub> concentrations produced by TS and SC, without and with ES, in open and closed systems together, as shown in figure 5. We averaged the measured concentrations for each discharge regime and the reactor type, which allows us to better compare these individual cases. Apparently, the closed reactor resulted in considerably higher (approximately one order of magnitude) concentrations of all measured species for both TS and SC. The closed reactor with a slow air flow rate enables accumulation of species, whereas immediate dilution of species with the surrounding ambient air occurs in the open reactor.

It is clear that SC in all systems generated lower NO and NO<sub>2</sub> (due to its lower power) but higher O<sub>3</sub> concentrations than TS. SC corresponds well to the low power ozone mode and TS to the high power NO<sub>x</sub> mode of the surface air DBD described by Pavlovich *et al* [12]. Power and air flow dependent formations of O<sub>3</sub> versus NO and NO<sub>2</sub> by corona-DBD air discharge were also described [61]. O<sub>3</sub> was completely absent in our NO<sub>x</sub>-dominated TS without water and in TS or TS-ES in the closed reactor. Very low O<sub>3</sub> concentrations were produced only in TS-ES (i.e. with water) that may be possibly explained by the TS discharge cooling by water evaporation that slowed down the O<sub>3</sub> thermal decomposition, or by a fast dilution of the small amount of produced O<sub>3</sub> that prevented it from depletion by reacting with NO (equation (9)). Understanding and assessing the roles of these effects requires further investigations.

Lower NO was produced in the systems with water, both in open and closed reactor (figure 5). As was discussed previously, this is mainly due to the NO dissolution into water (which is in agreement with our previously published results [37]). In the closed reactor where high NO<sub>2</sub> concentrations were generated, NO<sub>2</sub> was lowered by dissolution in the water ES, too. On the other hand, slightly higher NO<sub>2</sub> was produced in TS-ES compared with the TS without water in the open reactor, in agreement with the results shown in figure 4(b) and the corresponding discussion therein.

SC in the closed reactor produced negligible NO concentrations, lower than in the open reactor. At the same time, there was considerably more O<sub>3</sub> produced by SC in the closed reactor than in the open one. The reaction of NO oxidation by O<sub>3</sub> (equation (9)) probably depleted most of the generated NO that was oxidized to NO<sub>2</sub>, while the excess O<sub>3</sub> remained in the gas, which is also evident from figure 5.

In SC-ES in the open reactor, however, NO and NO<sub>2</sub> were approximately equal, despite the excess O<sub>3</sub> concentration. Perhaps faster air circulation and dilution in the open reactor saved some of the NO from its oxidation with O<sub>3</sub> to NO<sub>2</sub> if compared with the closed reactor, but this requires further investigations.

It is interesting to calculate the *net production rates of species* (NO, NO<sub>2</sub> and O<sub>3</sub>) expressed in nmol (i.e. number of molecules) per joule of dissipated energy in the gas volume, shown in figure 6. In this entire study, the discharge gases were pumped with a constant flow rate of 0.5 l min<sup>-1</sup>.

When the produced concentrations of gaseous species are normalized to per joule of energy, one can observe that SC is almost as efficient in NO<sub>2</sub> production rate as TS, and even more efficient in NO production rate in the open reactor with water ES. SC is much stronger in O<sub>3</sub> production rate in all cases, as it operates in the low power ozone mode. Therefore, SC, as the low power air discharge, is a very efficient RONS producer (per J) and is interesting for any biomedical applications, especially for small localized, thermally noninvasive treatments, such as wound healing, where very large concentrations of RONS are not needed. On the other hand, TS, which is about as efficient as SC in the production rate of NO<sub>x</sub> per J, is more convenient when higher NO<sub>x</sub> concentrations are needed, e.g. for PAW production, and when energy consumption is

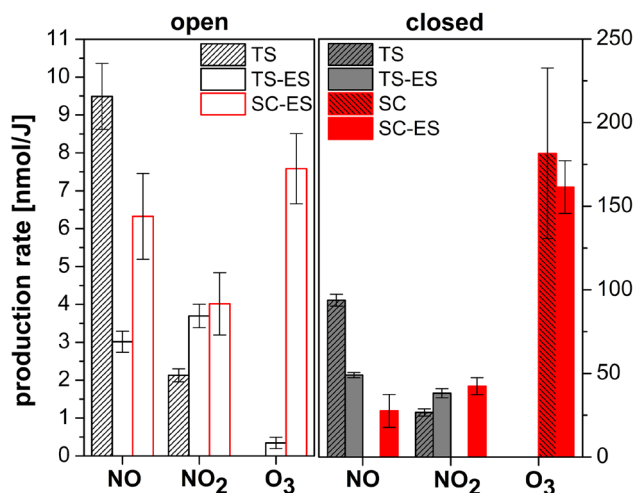


**Figure 6.** Net production rates of gaseous NO, NO<sub>2</sub> and O<sub>3</sub> expressed in nmol (i.e. number of molecules) per joule of dissipated energy in the gas by TS and SC discharges, without and with water ES, in open and closed (50 ml, 0.5 l min<sup>-1</sup> air flow) reactors. Statistical mean values with SEM.

not an issue (which is the case in most biomedical applications). Later in the manuscript we will look at these RONS concentrations versus energy aspects from the point of view of aqueous RONS production in PAW. Nonetheless, the same experimental system can be used to operate both TS and SC, according to the application requirements, and it is very easy to switch between two ballast and current-monitoring resistors, which make the only differences in the electrical circuit.

Figure 6 also shows that the NO production rate per J for TS without water compared with TS with water (TS-ES), was considerably higher, but not the NO<sub>2</sub> production rate (in both open and closed reactors). The closed reactor NO<sub>x</sub> production rate was about ten times higher than in the open reactor, and for O<sub>3</sub> production in SC it was even more. From the viewpoint of more efficient production of gaseous RONS, the closed reactor is certainly better in the absolute produced concentrations, as well as the production rate per J. In the closed reactor, O<sub>3</sub> production was slightly higher in SC (no water) than in SC-ES, probably due to the depletion of gaseous O<sub>3</sub> by dissolution in water enhanced by the electro-spray to fine droplets.

The maximum values of the net production rates for TS without water in the closed reactor were as high as 100 nmol J<sup>-1</sup> of NO and 30 nmol J<sup>-1</sup> of NO<sub>2</sub>. The total NO<sub>x</sub> = NO + NO<sub>2</sub> production rate corresponds to 8 × 10<sup>16</sup> molecules J<sup>-1</sup> (G-value ~ 1.3 molecules per 100 eV, or 80 eV/molecule), which is a relatively high NO<sub>x</sub> production rate and comparable with the hybrid glow-spark discharge or other reports [13, 41, 59].

It should be noted that the production rates mentioned above were calculated based on the measured concentrations of NO, NO<sub>2</sub> and O<sub>3</sub> by electrochemical sensors, UV absorption and FTIR absorption. The gas product diagnostics, however, was not immediate and *in situ* in the discharge, there was a certain delay given by the sampling air flow rate 0.5 l min<sup>-1</sup>, the lengths of the tubes and the time to make FTIR scans (approximately 30–60 s). Some of the NO and O<sub>3</sub> produced in

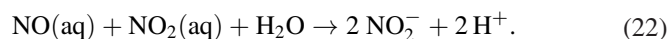
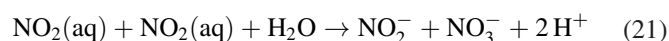
the discharge might have already been oxidized to NO<sub>2</sub> prior to or during the analysis, some of the gaseous products might have already been dissolved in the PAW, depending on their characteristic solubility, and some gaseous HNO<sub>2</sub> and HNO<sub>3</sub> (indeed detected as traces in the FTIR spectra) might have been formed and dissolved in the PAW. So the calculated ‘production rates’ do not exactly describe the actual production of species in the discharge but rather their ‘net production’ in the moment of the measurement. In addition, the speed of these reactions might have been different in both used discharges and the two tested reactors. In order to understand the chemical reactions and kinetics of species in more detail, further investigations including modeling are required.

### 3.4. Diagnostics and chemistry of PAW

We tested both air discharges, SC and TS, in water electro-spray treatment in both open and closed reactors and in this way prepared the PAW. We focused on the detection of long-lived aqueous RONS produced in PAW, namely H<sub>2</sub>O<sub>2</sub>, NO<sub>2</sub><sup>-</sup> and NO<sub>3</sub><sup>-</sup>, and dissolved O<sub>3</sub> by the two discharges, in open and closed systems. Clearly, the aqueous RONS concentrations are related to the plasma formed gaseous RONS.

Aqueous H<sub>2</sub>O<sub>2</sub>(aq) is produced by extremely fast dissolution of gaseous H<sub>2</sub>O<sub>2</sub>(g) formed in the gas by reaction (equation (12)) or other processes [30]. The Henry’s law solubility coefficient of H<sub>2</sub>O<sub>2</sub> ( $k_H \approx 9 \times 10^2 \text{ mol m}^{-3} \text{ Pa}^{-1}$ ) is about seven orders of magnitude larger than that of NO ( $\approx 1.9 \times 10^{-5} \text{ mol m}^{-3} \text{ Pa}^{-1}$ ) or NO<sub>2</sub> ( $\approx 1.2 \times 10^{-4} \text{ mol m}^{-3} \text{ Pa}^{-1}$ ) or O<sub>3</sub> ( $\approx 10^{-4} \text{ mol m}^{-3} \text{ Pa}^{-1}$ ) [46, 47], thus all H<sub>2</sub>O<sub>2</sub>(g) readily transfers into H<sub>2</sub>O<sub>2</sub>(aq) through the gas–liquid interface. Another possible mechanism of H<sub>2</sub>O<sub>2</sub>(aq) formation is directly in the liquid, by recombination of •OH radicals (equation (12) in an aqueous environment) or several other processes.

Nitrites NO<sub>2</sub><sup>-</sup> and nitrates NO<sub>3</sub><sup>-</sup> are generated in the PAW from the dissolved gaseous NO and NO<sub>2</sub> via the following reactions [10, 24, 62]:



The solubility coefficients of NO or NO<sub>2</sub> are much smaller than that of H<sub>2</sub>O<sub>2</sub> [46, 47], thus NO(g) and NO<sub>2</sub>(g) would not readily transfer into water to form NO<sub>2</sub><sup>-</sup>(aq) and NO<sub>3</sub><sup>-</sup>(aq). Enhancement of NO<sub>x</sub> dissolution by increasing the surface area of the plasma–liquid interface by spraying water into fine droplets in the ES system should be helpful.

Another way of producing NO<sub>2</sub><sup>-</sup>(aq) and NO<sub>3</sub><sup>-</sup>(aq) is a direct solvation of HNO<sub>2</sub>(g) and HNO<sub>3</sub>(g) with the immediate dissociation and H<sup>+</sup> release in the PAW for HNO<sub>3</sub> and pH-dependent dissociation of HNO<sub>2</sub> (pK<sub>a</sub> = 3.4). We were able to detect traces of gaseous HNO<sub>2</sub>(g) and HNO<sub>3</sub>(g) by FTIR but they were not quantified, so we are not able to assess to what extent these pathways contribute with respect to the above reactions (equations (21) and (22)). In every case, the Henry’s law solubility of HNO<sub>2</sub>(g) is high ( $k_H \approx 4.8 \times 10^{-1} \text{ mol m}^{-3} \text{ Pa}^{-1}$ ) and HNO<sub>3</sub>(g) extremely high ( $\approx 2.1 \times 10^3 \text{ mol m}^{-3} \text{ Pa}^{-1}$ ,

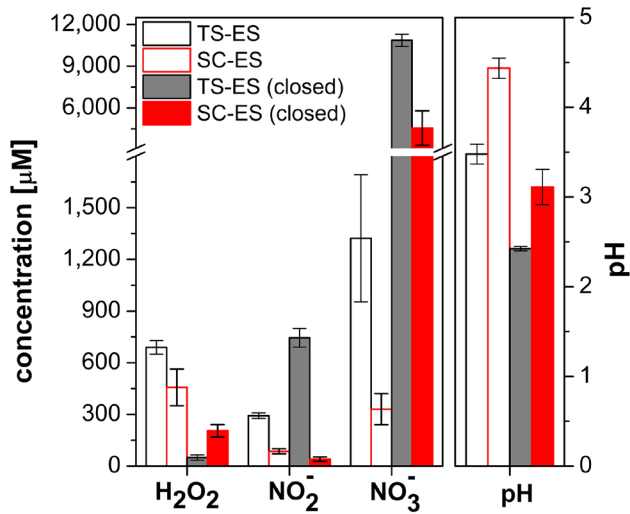
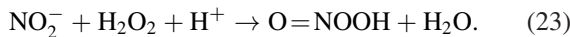


**Figure 7.** Concentrations of aqueous  $\text{H}_2\text{O}_2$ ,  $\text{NO}_2^-$ ,  $\text{NO}_3^-$  in PAW and corresponding pH for TS and SC with water ES, in the open and closed reactor. Statistical mean values with SEM.

comparable with  $\text{H}_2\text{O}_2$ ), so any  $\text{HNO}_2(\text{g})$  and  $\text{HNO}_3(\text{g})$  would readily dissolve in the PAW and enhance the  $\text{NO}_2^-$  and  $\text{NO}_3^-$  formation in the PAW.

Since protons  $\text{H}^+$  are released in the PAW by the above reactions, acidic pH is typical for PAW prepared by air plasmas.

The reaction between  $\text{H}_2\text{O}_2$  and  $\text{NO}_2^-$  occurs under acidic PAW conditions and leads to the formation of peroxyntrites (peroxynitrous acid) (equation (23),  $k = 1.1 \times 10^{-3} \text{ M}^{-2} \text{ s}^{-1}$  at pH 3.3) [10, 22, 24, 37]:



ONOOH then decomposes at acidic pH to  $\cdot\text{OH}$  and  $\cdot\text{NO}_2$  radicals (equation (24)) [24, 37]:

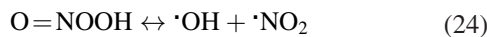
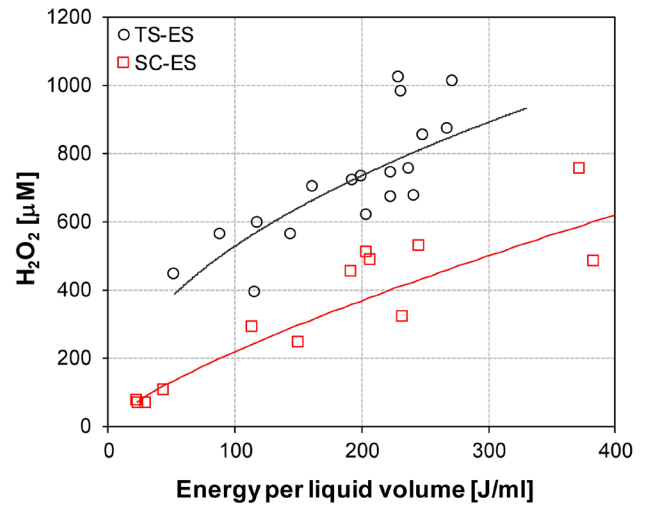


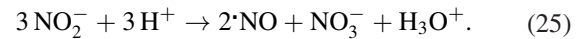
Figure 7 shows the measured concentrations of  $\text{H}_2\text{O}_2$ ,  $\text{NO}_2^-$ ,  $\text{NO}_3^-$  in PAW and corresponding pH for TS and SC with water ES in the open and closed reactor. The low power SC generates less  $\text{H}_2\text{O}_2$  and much less  $\text{NO}_2^- + \text{NO}_3^-$ , the ratio of  $\text{H}_2\text{O}_2/\text{NO}_2^-$  is approximately 6 in both the open and closed reactors. The character of this PAW produced in SC is similar to the one treated by low power surface DBD [12]. The higher power TS generates both  $\text{H}_2\text{O}_2$  and  $\text{NO}_2^- + \text{NO}_3^-$ , with the ratio of  $\text{H}_2\text{O}_2/\text{NO}_2^-$  approximately 2 in the open system. The character of this PAW is similar to those treated by pulsed multi-channel discharge or higher power surface DBD [12, 17, 24, 25]. On the other hand, after TS water activation in the closed system, much less  $\text{H}_2\text{O}_2$  and much more  $\text{NO}_2^-$  (ratio of  $\text{H}_2\text{O}_2/\text{NO}_2^-$  approximately 1/300) and particularly high  $\text{NO}_3^-$  were detected, which resulted in a very acidic pH (2.4). In addition, the water temperature was slightly increased from the room temperature (23 °C) to about 30 °C in this TS treatment in the closed reactor. The decreased pH by 1, and increased temperature, should have certainly accelerated the reactions (equations (23) and (24)). Their rate constant might have increased by as much as one order of magnitude [63].



**Figure 8.** Aqueous  $\text{H}_2\text{O}_2$  concentration in PAW as a function of energy density (energy deposited in liquid volume), open reactor, TS and SC with water ES.

So, the resulting  $\text{H}_2\text{O}_2$  measured after TS treatment was low due to depletion of  $\text{H}_2\text{O}_2$  with  $\text{NO}_2^-$  by these very fast reactions before  $\text{H}_2\text{O}_2$  was actually analyzed and measured after treatment. In such a case, the antibacterial effects might have been enhanced.

$\text{NO}_2^-$  was higher in TS than SC, and mostly increased with energy density per water volume. Closed TS resulted in very high  $\text{NO}_2^-$  and  $\text{NO}_3^-$ . It should be noted that the  $\text{NO}_2^-$  to  $\text{NO}_3^-$  disproportionation reaction is also pH-dependent and occurs faster at acidic pH < 3.5 (equation (25)) [24, 62]:



This reaction might have also contributed to the depletion of  $\text{NO}_2^-$  and have enhanced the final concentrations of  $\text{NO}_3^-$ , especially in the TS in the closed reactor where pH = 2.4.

SC in the closed reactor also generated high  $\text{NO}_3^-$  (yet lower than TS-ES closed) at pH 3.1, while very low  $\text{NO}_2^-$ . This might possibly be due to the  $\text{NO}_2^-$  depletion with ozone (equation (26)).



The rate constant of this reaction is fast ( $\sim 10^5 \text{ M}^{-1} \text{ s}^{-1}$ ) in the acidic pH [64].

$\text{H}_2\text{O}_2(\text{aq})$  concentration as a function of energy density (energy deposited in water volume) is shown in figure 8.  $\text{H}_2\text{O}_2(\text{aq})$  generally increased with the energy density. As the key process of  $\text{H}_2\text{O}_2$  formation is  $\cdot\text{OH}(\text{g})$  radical formation by water dissociation, the increasing trend with the energy density was expected and agrees with other published studies [27, 31, 32]. Anderson *et al* confirmed in experiments using indigo carmine as an indicator of oxidative strength in a similar air TS discharge that the activity of  $\cdot\text{OH}$  near the plasma–liquid interface dominates the effects of the plasma treatment. This result highlights the importance of gas plasma–liquid transport phenomena [27].

$\text{H}_2\text{O}_2$  is dominantly formed from  $\cdot\text{OH}$  radicals in the gas [45] and solvates extremely quickly (very high Henry's law solubility coefficient  $k_{\text{H}} \approx 9 \times 10^2 \text{ mol m}^{-3} \text{ Pa}^{-1}$  [46, 47]). We should note that in the ES, there is a good gas–liquid

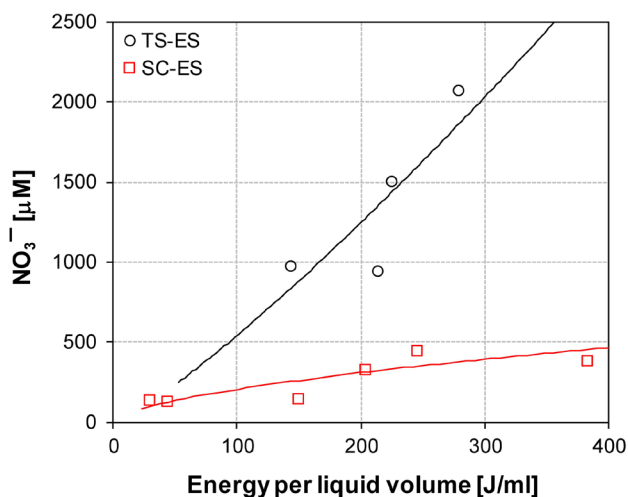


**Figure 9.** Aqueous  $\text{NO}_3^-$  concentration in PAW as a function of energy density (energy deposited in liquid water volume), open reactor, TS and SC with water ES.

mixing that might enhance the aqueous peroxytrite chemistry (equations (25) and (26)), which would then deplete the produced  $\text{H}_2\text{O}_2(\text{aq})$  faster. The measured  $\text{H}_2\text{O}_2(\text{aq})$  concentrations after treatment may then be lower with respect to the  $\text{H}_2\text{O}_2(\text{aq})$  really produced during the plasma–water interaction.

Similar to  $\text{H}_2\text{O}_2$ ,  $\text{NO}_3^-(\text{aq})$  concentration as a function of energy density (energy deposited in water volume) in the open reactor is shown in figure 9. Aqueous  $\text{NO}_3^-$  increased with the energy density in both discharges.  $\text{NO}_3^-$  were higher for TS than SC, which can be certainly related with considerably higher gaseous NO and  $\text{NO}_2$  production in the TS (figure 5).

$\text{O}_3(\text{aq})$  concentrations in PAW increased as a function of energy density in the open reactor with SC-ES. Dissolved ozone concentrations  $\text{O}_3(\text{aq})$  in PAW were detected with at least some degree of reliability in SC. There was almost negligible gaseous  $\text{O}_3$  detected in TS, and consequently undetectable  $\text{O}_3$  dissolved in PAW either. We have previously showed that the well established indigo blue colorimetric assay of dissolved  $\text{O}_3$  might be misleading in PAW, especially treated by the air TS where peroxytrite chemistry takes place and the indigo blue dye is bleached not only by  $\text{O}_3$  but also by other ROS, most likely  $\bullet\text{OH}$  radicals [37]. However, we should note that the peroxytrite chemistry could have also partly occurred in SC-ES. Therefore, the indigo blue assay that was used to detect  $\text{O}_3(\text{aq})$  might have overestimated the real  $\text{O}_3(\text{aq})$  concentration, although not as much as in TS-ES. Looking for an alternative method of aqueous  $\text{O}_3$  measurement in PAW free of interactions with other ROS (especially  $\bullet\text{OH}$ ) will be our future objective.

It is noteworthy that TS discharge generates high concentrations of O atoms. According to some recent studies performed with atmospheric pressure plasma jets in He/ $\text{O}_2$  mixtures [65, 66], gaseous  $\bullet\text{O}$  radicals can dissolve into water and influence the aqueous chemistry. The question whether this  $\bullet\text{O}(\text{aq})$  would be present in air plasma–water interface where the RONS chemistry is more complex both in the gas and aqueous phase, is to be investigated further.

There is no doubt that other RONS except those measured and discussed above ( $\text{H}_2\text{O}_2$ ,  $\text{NO}_2^-$ ,  $\text{NO}_3^-$ ,  $\text{O}_3$ ,  $\text{ONOOH}$ ) may contribute to important processes in the PAW and the antibacterial effects. For example, Ikawa *et al.* indirectly evidenced peroxytrite acid ( $\text{O}_2\text{NOOH}$ ) in PAW, besides other active RONS, based on the reaction kinetics analysis [67]. To the best of our knowledge there are no known methods of direct measurement of low concentrations of  $\text{O}_2\text{NOOH}$  in aqueous solutions.  $\text{O}_2\text{NOOH}$ , which is a stronger acid than  $\text{ONOOH}$  ( $\text{pK}_a = 5.9$ ), is formed both in the gas and water by the reaction of  $\text{HO}_2^\bullet$  (or  $\text{O}_2^{\bullet-}$  according to pH) +  $\bullet\text{NO}_2$ , and decays back to the same radicals (so it may be a potential source of  $\text{HO}_2^\bullet$  in PAW) [68]. Certainly, we cannot rule out the potential occurrence and role of  $\text{O}_2\text{NOOH}$  co-acting with  $\text{ONOOH}$  but we have no experimental evidence of  $\text{O}_2\text{NOOH}$ . On the other hand, the measured stable species that lead to  $\text{ONOOH}$  chemistry correlate well with our antibacterial effects. Rigorous considering and detecting  $\text{O}_2\text{NOOH}$  will require further research.

Superoxide anion  $\text{O}_2^{\bullet-}$ , known to have many biological functions in cell biochemistry, is another example of RONS that we did not detect. It is likely formed by the attachment of slow electrons to  $\text{O}_2$  molecules in our air plasma discharges but  $\text{O}_2^{\bullet-}$  concentration in the gas decays dramatically within a few tens of microseconds, so it is unlikely that it could be directly transported into water. Its main channel of formation in the aqueous environment is by the decay of peroxytrites  $\text{ONOO}^- \rightarrow \bullet\text{NO} + \text{O}_2^{\bullet-}$ . However, in our PAW with acidic pH < 4.8 ( $\text{pK}_a$  of  $\text{O}_2^{\bullet-}/\text{HO}_2^\bullet$  ionic/acidic forms), the dominant form is  $\text{HO}_2^\bullet$  (and the dominant form is  $\text{ONOOH}$  not  $\text{ONOO}^-$ , too,  $\text{pK}_a = 6.8$ ), so  $\text{O}_2^{\bullet-}$  form is unlikely to be present. Unfortunately, there are very limited possibilities of measuring  $\text{O}_2^{\bullet-}$  (or  $\text{HO}_2^\bullet$ ) in aqueous solutions besides spin-trapping EPR which was not available for this study.

Figure 10 shows a diagram indicating important species generated as a result of the predominant air plasma gaseous and aqueous reactions, including transport from plasma to water driven by species-specific Henry's law solubility coefficients. The diagram includes only the species and corresponding reactions that are mentioned and referred to in the text of the paper. We admit it may not be a complete picture of the real processes but it is based on the experimentally measured species, the most probable mechanisms of their formations and their interactions.

### 3.5. Production rate of total aqueous and gaseous RONS

In air plasma chemistry, NO (and also  $\text{N}_2\text{O}$ ) eventually become oxidized to  $\text{NO}_2$ , which is the final oxidation product. In aqueous  $\text{NO}_x$  chemistry,  $\text{NO}_2^-$  get oxidized to  $\text{NO}_3^-$ , which is also the final oxidation product. Since our liquid diagnostics methods are post-treatment and even the online gas diagnostics have a certain time delay given the air flow rate  $0.5 \text{ l min}^{-1}$  and the lengths of the tubes (approximately 30 s), some of the NO might have already been oxidized to  $\text{NO}_2$ , as well as some  $\text{NO}_2^-$  into  $\text{NO}_3^-$  in the PAW, in the moment when they were measured. In addition, the speed of these reactions

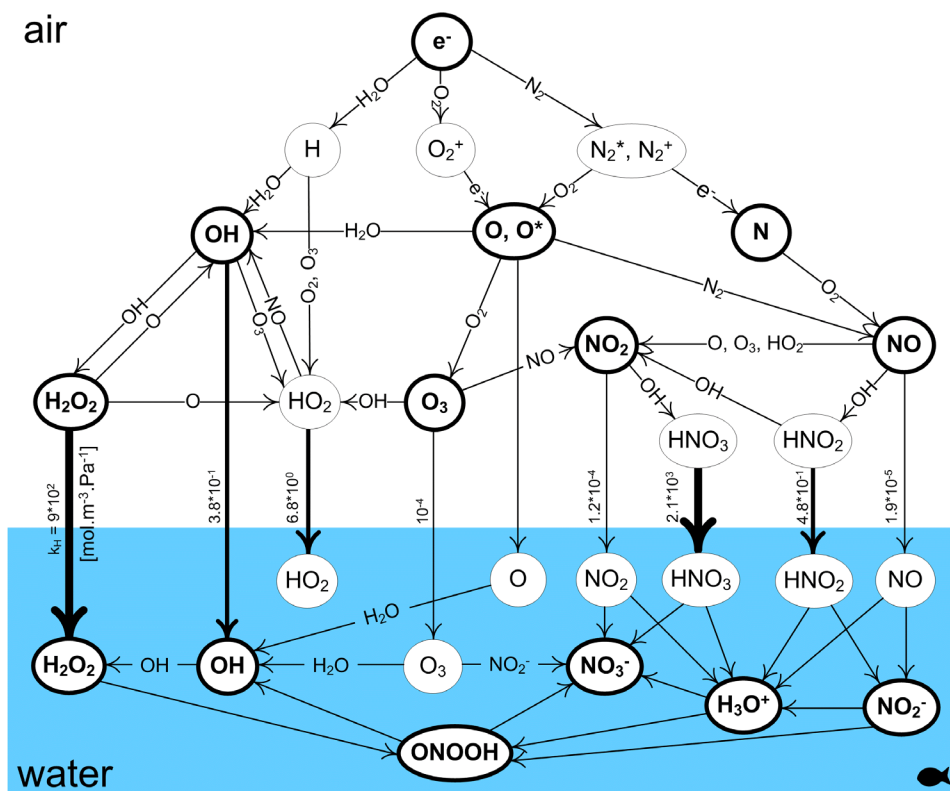


**Figure 10.** Schematic diagram indicating important species generated as a result of the predominant air plasma gaseous and aqueous reactions, including transport from plasma to water driven by species-specific Henry’s law solubility coefficients. The most important species are in bold.

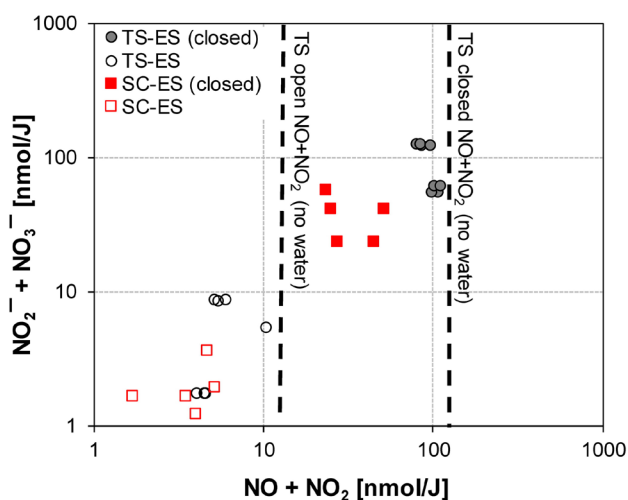


**Figure 11.** Correlation of the net production rate of total aqueous  $\text{NO}_x^-$  (represented as  $\text{NO}_2^- + \text{NO}_3^-$  produced moles per J of energy dissipated in water) as a function of the total gaseous  $\text{NO}_x$  (represented as  $\text{NO} + \text{NO}_2$  produced moles per J of energy dissipated in air). TS and SC with water ES, in the open and closed reactor. Log–log scale. Two vertical lines show the total  $\text{NO} + \text{NO}_2$  production rates for TS without water, open and closed reactor.

might have been different in the two discharges and the two tested reactors. Therefore, it makes sense to express the total aqueous  $\text{NO}_x^-$  (aq) against the total gaseous  $\text{NO}_x$ (g) produced. Figure 11 correlates the production rate of total aqueous  $\text{NO}_x^-$  (aq) (represented as  $\text{NO}_2^- + \text{NO}_3^-$  produced moles per J of energy dissipated in water) as a function of the total gaseous  $\text{NO}_x$ (g) (represented as  $\text{NO} + \text{NO}_2$  produced moles per

J of energy dissipated in air). We are not accounting for other gaseous  $\text{NO}_x$  such as  $\text{N}_2\text{O}$  (very low concentrations, detectable only in the closed reactor: 5–15 ppm), and  $\text{HNO}_2$  and  $\text{HNO}_3$  (traces detected in the FTIR spectra but not quantified).

Regardless of the discharge regime, the water introduction by ES and the reactor type (open versus closed), there is a very good correlation of the production rate of the total aqueous  $\text{NO}_x^-$  (aq) (represented as  $\text{NO}_2^- + \text{NO}_3^-$ ) and the production rate of the total gaseous  $\text{NO}_x$ (g) ( $\text{NO} + \text{NO}_2$ ). Despite the fact that the ratio of gaseous  $\text{NO}$  and  $\text{NO}_2$  was different in TS without and with water, their sum, i.e. the total  $\text{NO}_x$ (g), were lower in TS-ES than in TS without water both in the open and closed reactors (open and closed black points are lower on the x-axis than the two indicated vertical lines). TS  $\text{NO}_x$  production rates were higher compared to SC, both in the open and closed reactor. The closed reactor enabled higher production rates of both gaseous and aqueous  $\text{NO}_x$  than the open one. In summary, the total gaseous  $\text{NO}_x$ (g) production rate determines the total aqueous  $\text{NO}_x^-$  (aq) production rate for both studied discharges and reactors and one can select the most suitable discharge and reactor based on the required  $\text{NO}_x$ (g) and  $\text{NO}_x^-$  (aq) production.

To summarize this part on aqueous RONS in the PAW, we expressed their net production rates per joule of deposited energy in the water volume in  $[\text{nmol J}^{-1}]$ , as shown in figure 12 in a similar way to how we expressed the net production rates of gaseous products in figure 6. SC was operated at much lower power than TS and produced considerably lower RONS concentrations (as shown e.g. in figure 7), but its

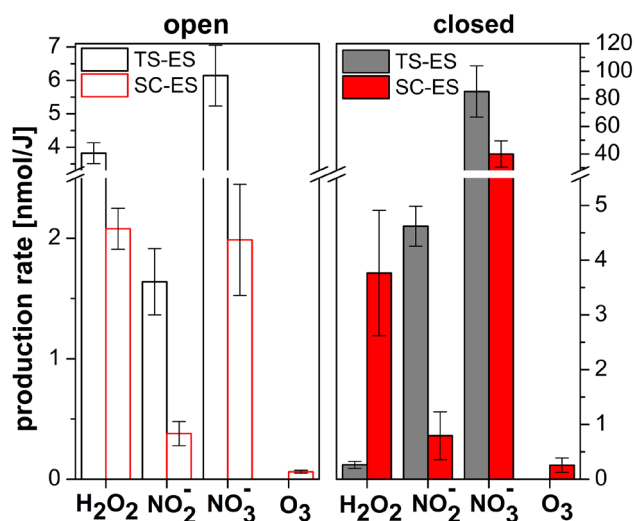


**Figure 12.** Production rates of aqueous H<sub>2</sub>O<sub>2</sub>, NO<sub>2</sub><sup>-</sup>, NO<sub>3</sub><sup>-</sup> and O<sub>3</sub> in PAW with respect to the energy density dissipated in liquid volume for TS and SC with water ES, in the open and closed reactor. Statistical mean values with SEM.

production rates of H<sub>2</sub>O<sub>2</sub>, NO<sub>2</sub><sup>-</sup> and NO<sub>3</sub><sup>-</sup> per joule in the open reactor were only somewhat lower than in TS. In the closed reactor, SC produced significantly higher H<sub>2</sub>O<sub>2</sub> than TS but lower NO<sub>2</sub><sup>-</sup> and NO<sub>3</sub><sup>-</sup>. However, as we previously discussed, following the reactions (equations (23) and (24)), the actual production of H<sub>2</sub>O<sub>2</sub> in TS-ES in the closed reactor might have been much higher before H<sub>2</sub>O<sub>2</sub> was sampled and measured after treatment, since it was probably quickly depleted by the reaction with NO<sub>2</sub><sup>-</sup> in very acidic conditions.

### 3.6. Antibacterial effects induced directly in PAW

Besides extensive analysis of the gaseous products of the two air discharges in two types of reactors and related aqueous RONS formed in the PAW, we examined the most typical application of PAW—its antibacterial effects in relation to the gaseous and aqueous RONS. Inactivation efficiency of *E. coli* bacteria suspended in the water treated by both plasma discharges in ES in both open and closed reactors was correlated with the RONS generation in water.

Figure 13 shows the antibacterial PAW effect tested in *E. coli* bacterial log reduction as a function of the energy density. One can see that the effect increased with the energy density, in a similar trend as with H<sub>2</sub>O<sub>2</sub> or NO<sub>3</sub><sup>-</sup> (figures 8 and 9). Clearly, the SC effect was much weaker than that of TS.

Figure 14 provides a closer look at the antibacterial effect as a function of the discharge (TS versus SC), open versus closed reactor and various water ES flow rates. In the open reactor, for both TS and SC discharge, the antibacterial effect decreased when the water flow rate (in ES) increased. In agreement with figure 13, TS-ES was more efficient against bacteria than SC-ES.

In the closed reactor, all flow rates of both TS-ES and SC-ES resulted in a full bacterial inactivation (6.1 logs, maximum limit of the experiment based on the initial bacterial population in water), despite the fact that the concentrations

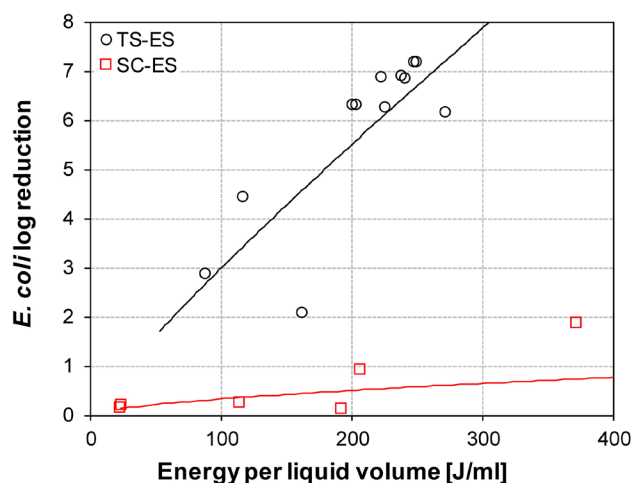


**Figure 13.** Antibacterial effect in PAW tested on *E. coli* log reduction as a function of energy density (energy deposited in liquid water volume), open reactor, TS and SC with water ES.

and production rates of RONS varied depending on the discharge and water flow rate. However, we should note that the temperature of the PAW has been slightly increased by the discharge in the closed reactor, especially with TS (up to 30 °C), and the pH has dropped very low (pH = 2.4 in TS-ES and 3.1 in SC-ES). The ONOOH formation and decay mechanisms were probably strongly accelerated, as discussed above [63]. In addition, there were very high NO<sub>3</sub><sup>-</sup> and at such acidic pH < pK<sub>a</sub> of HNO<sub>2</sub>/NO<sub>2</sub><sup>-</sup> would be completely in the form of HNO<sub>2</sub>, or so called acidified nitrite, which is also known for its antibacterial [3, 9] and antiviral [20] effects. So, these strong antibacterial effects observed in the closed reactor were most likely due to antibacterial ONOOH formation and decay combined with the effect of acidified nitrite.

On the other hand, the antibacterial effects obtained by TS-ES in the open reactor where the PAW temperature after plasma treatment stayed ambient (<25 °C) and pH ~ 3.3, were mainly due to the NO<sub>2</sub><sup>-</sup> interaction with H<sub>2</sub>O<sub>2</sub> in acidic conditions (equations (23) and (24)) promoting peroxyxynitrous acid (ONOOH) formation and its consequent decay to •OH and other radicals. ONOO<sup>-</sup>/ONOOH were identified as the most important antibacterial RONS agents in the TS-PAW previously [10, 16, 21, 22, 24, 26, 28].

In SC, the bacterial log reduction rate is relatively high despite NO<sub>2</sub><sup>-</sup> concentration being very low compared to H<sub>2</sub>O<sub>2</sub> which would again slow down the ONOOH formation and its antibacterial action. Aqueous O<sub>3</sub> most likely contributed to the overall antibacterial action in SC (unlike in TS).

We correlated and explained the key gaseous RONS, their transport to water and the consequent aqueous RONS chemistry in PAW with related antibacterial effects. Besides RONS chemistry, other plasma agents may likely play roles, e.g. electric fields, UV radiation and heat. Electric field may influence the bacterial cells enclosed in charged electrosprayed water droplets passing through the discharge. UV radiation is well known to be antibacterial, especially UV C. Based on our emission spectroscopy studies, SC and the streamer phase of TS do not emit any considerable UV B and UV C and even very low UV A radiation. The TS spark phase emission

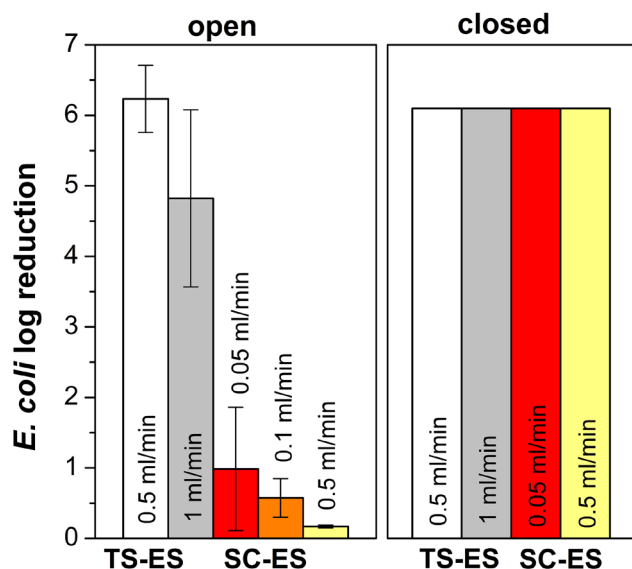


**Figure 14.** Antibacterial effect tested on *E. coli* log reduction as a function of the TS versus SC discharge, open-closed reactor, ES with various water flow rates. Statistical mean values with SEM.

dominated by atomic  $\bullet\text{O}$ ,  $\bullet\text{N}$ ,  $\bullet\text{H}$  in the visible region emits some NO gamma radiation in UV C-B that might contribute to antibacterial effects. However, based on our previous study [8], the intensity of this UV emission from TS was so low that the effect on bacteria was negligible. Finally, despite the fact that instantaneous gas temperatures in the TS spark phase can reach  $>1000\text{K}$  for the extremely short period of several tens of ns, the effect of the PAW heating up to about  $30\text{ }^\circ\text{C}$  was only detected in the TS in the closed reactor, while in all other cases the PAW remained at room temperature.  $T = 30\text{ }^\circ\text{C}$  is too low to harm bacteria directly; however, it might have an effect on accelerating the chemical processes of ONOOH formation and decay, which might have contributed to the strong antibacterial effects in the closed reactor, as already discussed above. Investigations of the effects of the electric field, UV and heat separated from RONS chemistry will be a subject of our future studies.

Based on all these arguments we believe that the conclusions drawn from the experimental results in this article based on gaseous RONS, their species-specific transport into water and consequent aqueous RONS chemistry, and their relation to antibacterial effects, are correct in general.

#### 4. Conclusions

The potential use of PAW and liquids is constantly growing in various biomedical and agricultural applications. The chemical properties and effects of PAW strongly depend on the plasma sources and discharge regimes used and their interaction with water. The key objective of this article is to understand the atmospheric air plasma chemistry and its relation to the properties of PAW and subsequent antibacterial effects. Understanding these relations would enable a better control and tailoring of PAW generation by air plasmas, and

their properties and effects depending on the desired applications. We compared two nonthermal atmospheric plasma sources operating in air and interacting with water: a lower power streamer corona (SC, 0.4 W) and a higher power transient spark (TS, 2 W). We analyzed their gaseous and aqueous RONS in the air and the PAW, and their antibacterial effects were tested on *E. coli* bacteria in water. Water was activated in the ES to fine aerosol droplets sprayed through the plasma zone. We also compared the open air and closed small volume reactor at different air flow rates to understand the effects of reactor volume and air flow rate on the gaseous and aqueous chemistry. Gaseous discharge product concentrations were measured by electrochemical sensors, UV absorption and FTIR absorption spectroscopy. Aqueous RONS were diagnosed by UV absorption spectroscopy using colorimetric assays. Antibacterial effects were determined from microbial cultivation of *E. coli*.

In air plasmas, the generation of NO and  $\text{NO}_2$  is governed by a sequence of elementary plasma processes. Excited  $\text{N}_2^*$  molecules are produced by the high energy electron impact of the streamer and spark current pulses. They, together with direct  $\text{O}_2$  dissociation, lead to the significant amounts of atomic oxygen radicals necessary for the synthesis of NO or  $\text{O}_3$ . NO is oxidized to  $\text{NO}_2$  by additional  $\bullet\text{O}$ , as well as by the reaction with  $\text{O}_3$ . In discharges with water (especially in the ES),  $\text{H}_2\text{O}$  molecules are dissociated by electron impact and produce  $\bullet\text{OH}$  or  $\text{HO}_2^\bullet$  radicals, resulting in  $\text{H}_2\text{O}_2(\text{g})$  that interact with NO and  $\text{NO}_2$  and influence their measured gas-phase concentrations and lead to  $\text{HNO}_2(\text{g})$  and  $\text{HNO}_3(\text{g})$  formation. Gaseous  $\text{H}_2\text{O}_2$ ,  $\text{HNO}_2$  and  $\text{HNO}_3$  are readily dissolved in water due to their high solubilities, resulting in aqueous  $\text{H}_2\text{O}_2$ , nitrites  $\text{NO}_2^-$  and nitrates  $\text{NO}_3^-$  and acidification of the PAW. Gaseous NO and  $\text{NO}_2$  also dissolve in water and contribute to the formation of  $\text{NO}_2^-$  and  $\text{NO}_3^-$  and acidic pH.  $\text{H}_2\text{O}_2$  and  $\text{NO}_2^-$  react in PAW under acidic conditions to form intermediate peroxyxynitrous acid (ONOOH) that eventually decay into  $\bullet\text{OH}$  and  $\bullet\text{NO}_2$  radicals responsible for the strong antibacterial effects.

Low power streamer corona air discharge produced considerable  $\text{O}_3$ , besides low NO and  $\text{NO}_2$  concentrations. With water electro spray, some of this  $\text{O}_3(\text{g})$  is transferred into the PAW and contributes to the antibacterial action, in addition to the effect of aqueous  $\text{H}_2\text{O}_2$  and  $\text{NO}_2^-$  that were detected in the mildly acidic SC-PAW as well.

In higher power transient spark,  $\text{O}_3$  formation is suppressed and the gas products are dominated by NO and  $\text{NO}_2$ . With water ES, NO(g) concentrations decrease due to NO dissolution in water and gas temperature decrease in the TS channel.  $\text{NO}_2(\text{g})$  slightly increased with water ES due to its enhanced oxidation by  $\bullet\text{O}$ ,  $\text{HO}_2^\bullet$  or  $\text{O}_3$  to  $\text{NO}_2$ . Strong antibacterial effects in the PAW are predominantly due to the aqueous  $\text{H}_2\text{O}_2(\text{aq})$  and  $\text{NO}_2^-(\text{aq})$  at acidic pH leading to ONOOH formation and its decay to  $\bullet\text{OH}$  and  $\bullet\text{NO}_2$  radicals in the PAW.

All gaseous RONS in both SC and TS were considerably higher in the closed reactor with respect to the open air reactor, due to the accumulation of species, and because the sampled gas was diluted by the surrounding ambient air in the open reactor. The aqueous  $\text{NO}_2^-$  and especially  $\text{NO}_3^-$  concentrations

were also significantly higher in the closed reactor and the corresponding PAW was more acidified by the discharge. The low pH and high  $\text{NO}_2^-$  (i.e. acidified nitrite—nitrous acid  $\text{HNO}_2$ ) and  $\text{NO}_3^-$  might have contributed to the strong antibacterial effects induced by the ONOOH mechanism.

Calculating the net production rates of gaseous and aqueous RONS per joule of energy dissipated in the gas or liquid volume enabled us to better compare the two discharge regimes (TS and SC) that operated at different powers. Interestingly, the net production rates (per joule) of NO and  $\text{NO}_2$  of the low power SC were almost as high as those of higher power TS. SC was much stronger in the  $\text{O}_3$  production rate (per joule). In aqueous RONS production, TS produced about twice as much  $\text{H}_2\text{O}_2$  in the open reactor but less  $\text{H}_2\text{O}_2$  in the closed reactor (per joule). Production rates of  $\text{NO}_2^-$  and  $\text{NO}_3^-$  were higher in TS than in SC, especially in the closed reactor. Plotting the total aqueous  $\text{NO}_x$  ( $\text{NO}_2^- + \text{NO}_3^-$ ) production rate against the total gaseous  $\text{NO}_x$  production rate ( $\text{NO} + \text{NO}_2$ ) gave an approximately linear dependence. This indicates that the production of aqueous RONS is determined by the gaseous plasma products. It also shows that the total  $\text{NO}_x$  production in TS was slightly higher than in SC, and that the closed reactor production rate was about ten times higher for both discharges than that for the open reactor.

Antibacterial effects in the water air plasma-ES treatment strongly depend on the reactor type, discharge regime, as well as the water flow rate. The faster water flow rate reduced the effects (in the open reactor). TS was more efficient than SC, especially due to the higher produced concentrations of aqueous RONS. The closed reactor resulted in the maximum antibacterial effect (6.1 logs) detectable in our experiments for both SC and TS and all flow rates. The effect might have been due to much higher aqueous RONS concentrations (including higher dissolved  $\text{O}_3$  in SC), as well as the lower pH and slightly increased temperature of the PAW. The closed reactor would therefore be recommended in applications where higher RONS concentrations and lower pH of the PAW are not an issue (e.g. wastewater cleaning and disinfection). Nevertheless, it is noteworthy that the open reactor TS-ES at a  $0.5 \text{ ml min}^{-1}$  water flow rate resulted in almost the same antibacterial effect ( $\sim 6.3$  logs), despite considerably lower aqueous RONS concentrations. This is probably due to an optimum ratio of  $\text{H}_2\text{O}_2/\text{NO}_2^- \approx 2$  and  $\text{pH} \sim 3.3$  which are very favorable for the ONOOH mechanism, and are most likely responsible for the antibacterial action of the air plasma PAW. For more delicate PAW applications (e.g. wound healing, dentistry or other *in vivo* applications) where too low pH and high  $\text{NO}_x$  (TS closed) or dissolved ozone (SC closed) may represent a problem, a better approach for preparing PAW would be using TS discharge in an open air reactor with the same antibacterial efficacy and lower RONS concentrations.

In summary, both SC and TS represent inexpensive and easy to operate nonequilibrium air plasma sources that can be run in the same versatile setup. Switching between them can be easily managed by changing the resistors in the circuit. Each of these discharge regimes generates air plasma with different properties resulting in different gaseous products: dominated by  $\text{O}_3$  in lower power SC and by  $\text{NO}_x$  in higher power TS. The gaseous

products, their production rates and their solvation determine the aqueous RONS in the activated water, which then control the antibacterial effects of such PAW. Gas flow conditions in the reactor strongly influence gaseous and aqueous RONS production. We applied water electrospray through the discharges as the efficient method of transfer of the plasma gaseous species into the PAW. Other methods of water interaction with air plasmas can lead to different transfer mechanisms of some species (especially those with low solubility), which may influence the aqueous chemistry and antibacterial effects and will be a subject of our future study.

## Acknowledgments

This work was supported by Slovak Research and Development Agency APVV-17-0382 and APVV-0134-12, and Slovak Grant Agency VEGA 1/0419/18. We thank Dr Michal Stano for the use of his NO electrochemical sensor, Professor Viktor Martišovič for his electrotechnical assistance and Richard Cimerman for his help with NO and  $\text{NO}_2$  calibration.

## ORCID iDs

Z Machala  <https://orcid.org/0000-0003-1424-1350>  
 B Tarabová  <https://orcid.org/0000-0001-9936-1786>  
 M Janda  <https://orcid.org/0000-0001-9051-4221>  
 K Hensel  <https://orcid.org/0000-0001-6833-681X>

## References

- [1] Bruggeman P J *et al* 2016 Plasma–liquid interactions: a review and roadmap *Plasma Sources Sci. Technol.* **25** 053002
- [2] Adamovich I *et al* 2017 The 2017 plasma roadmap: low temperature plasma science and technology *J. Phys. D: Appl. Phys.* **50** 323001
- [3] Graves D B 2012 The emerging role of reactive oxygen and nitrogen species in redox biology and some implications for plasma applications to medicine and biology *J. Phys. D: Appl. Phys.* **45** 263001
- [4] Lu X, Naidis G V, Laroussi M, Reuter S, Graves D B and Ostrikov K 2016 Reactive species in non-equilibrium atmospheric-pressure plasmas: generation, transport, and biological effects *Phys. Rep.* **630** 1–84
- [5] Bauer G and Graves D B 2016 Mechanisms of selective antitumor action of cold atmospheric plasma-derived reactive oxygen and nitrogen species *Plasma Process. Polym.* **13** 1157–78
- [6] Reuter S, von Woedtke T and Weltmann K 2018 The kINPen—a review on physics and chemistry of the atmospheric pressure plasma jet and its applications *J. Phys. D: Appl. Phys.* **51** 233001
- [7] Tanaka H *et al* 2014 Plasma medical science for cancer therapy: toward cancer therapy using nonthermal atmospheric pressure plasma *IEEE Trans. Plasma Sci.* **42** 3760–4
- [8] Machala Z, Chládková L and Pelach M 2010 Plasma agents in bio-decontamination by dc discharges in atmospheric air *J. Phys. D: Appl. Phys.* **43** 222001
- [9] Traylor M J, Pavlovich M J, Karim S, Hait P, Sakiyama Y, Clark D S and Graves D B 2011 Long-term antibacterial

- efficacy of air plasma-activated water *J. Phys. D: Appl. Phys.* **44** 472001
- [10] Machala Z, Tarabová B, Hensel K, Spetlikova E, Sikurova L and Lukeš P 2013 Formation of ROS and RNS in water electro-sprayed through transient spark discharge in air and their bactericidal effects *Plasma Process. Polym.* **10** 649–59
- [11] Pawlat J 2013 Atmospheric pressure plasma jet for decontamination purposes *Eur. Phys. J. Appl. Phys.* **61** 24323
- [12] Pavlovich M J, Clark D S and Graves D B 2014 Quantification of air plasma chemistry for surface disinfection *Plasma Sources Sci. Technol.* **23** 065036
- [13] Pavlovich M J, Ono T, Galleher C, Curtis B, Clark D S, Machala Z and Graves D B 2014 Air spark-like plasma source for antimicrobial NO<sub>x</sub> generation *J. Phys. D: Appl. Phys.* **47** 505202
- [14] Hensel K et al 2015 Effects of air transient spark discharge and helium plasma jet on water, bacteria, cells, and biomolecules *Biointerphases* **10** 029515
- [15] Kovalova Z, Leroy M, Kirkpatrick M J, Odic E and Machala Z 2016 Corona discharges with water electro-spray for *Escherichia coli* biofilm eradication on a surface *Bioelectrochemistry* **112** 91–9
- [16] Shen J, Tian Y, Li Y, Ma R, Zhang Q, Zhang J and Fang J 2016 Bactericidal effects against *S. aureus* and physicochemical properties of plasma activated water stored at different temperatures *Sci. Rep.* **6** 28505
- [17] Lu P, Boehm D, Bourke P and Cullen P J 2017 Achieving reactive species specificity within plasma-activated water through selective generation using air spark and glow discharges *Plasma Process. Polym.* **14** e1600207
- [18] Liu Z, Xu D, Liu D, Cui Q, Cai H, Li Q, Chen H and Kong M G 2017 Production of simplex RNS and ROS by nanosecond pulse N<sub>2</sub>/O<sub>2</sub> plasma jets with homogeneous shielding gas for inducing myeloma cell apoptosis *J. Phys. D: Appl. Phys.* **50** 195204
- [19] Modic M, McLeod N P, Sutton J M and Walsh J L 2017 Cold atmospheric pressure plasma elimination of clinically important single- and mixed-species biofilms *Int. J. Antimicrob. Agents* **49** 375–8
- [20] Nayak G, Aboubakr H A, Goyal S M and Bruggeman P J 2017 Reactive species responsible for the inactivation of feline calicivirus by a two-dimensional array of integrated coaxial microhollow dielectric barrier discharges in air *Plasma Process. Polym.* **15** e1700119
- [21] Ke Z, Thopan P, Fridman G, Miller V, Yu L, Fridman A and Huang Q 2017 Effect of N<sub>2</sub>/O<sub>2</sub> composition on inactivation efficiency of *Escherichia coli* by discharge plasma at the gas-solution interface *Clin. Plasma Med.* **7–8** 1–8
- [22] Brisset J-L and Hnatiuc E 2012 Peroxynitrite: a re-examination of the chemical properties of non-thermal discharges burning in air over aqueous solutions *Plasma Chem. Plasma Process.* **32** 655–74
- [23] Tresp H, Hammer M U, Winter J, Weltmann K-D and Reuter S 2013 Quantitative detection of plasma-generated radicals in liquids by electron paramagnetic resonance spectroscopy *J. Phys. D: Appl. Phys.* **46** 435401
- [24] Lukeš P, Dolezalova E, Sisrova I and Clupek M 2014 Aqueous-phase chemistry and bactericidal effects from an air discharge plasma in contact with water: evidence for the formation of peroxynitrite through a pseudo-second-order post-discharge reaction of H<sub>2</sub>O<sub>2</sub> and HNO<sub>2</sub> *Plasma Sources Sci. Technol.* **23** 015019
- [25] Laurita R, Barbieri D, Gherardi M, Colombo V and Lukeš P 2015 Chemical analysis of reactive species and antimicrobial activity of water treated by nanosecond pulsed DBD air plasma *Clin. Plasma Med.* **3** 53–61
- [26] Brisset J L and Pawlat J 2016 Chemical effects of air plasma species on aqueous solutes in direct and delayed exposure modes: discharge, post-discharge and plasma activated water *Plasma Chem. Plasma Process.* **36** 355–81
- [27] Anderson C E, Cha N R, Lindsay A D, Clark D S and Graves D B 2016 The role of interfacial reactions in determining plasma-liquid chemistry *Plasma Chem. Plasma Process.* **36** 1393–415
- [28] Girard F, Badets V, Blanc S, Gazeli K, Marlin L, Authier L, Svarnas P, Sojic N, Clément F and Arbault S 2016 Formation of reactive nitrogen species including peroxynitrite in physiological buffer exposed to cold atmospheric plasma *RSC Adv.* **6** 78457–67
- [29] Gorbanev Y, O'Connell D and Chechik V 2016 Non-thermal plasma in contact with water: the origin of species *Chem.—Eur. J.* **22** 3496–505
- [30] Hsieh K C, Wandell R J, Bresch S and Locke B R 2017 Analysis of hydroxyl radical formation in a gas-liquid electrical discharge plasma reactor utilizing liquid and gaseous radical scavengers *Plasma Process. Polym.* **14** e1600171
- [31] Chauvin J, Judée F, Yousfi M, Vicendo P and Merbahi N 2017 Analysis of reactive oxygen and nitrogen species generated in three liquid media by low temperature helium plasma jet *Sci. Rep.* **7** 4562
- [32] Ito T, Uchida G, Nakajima A, Takenaka K and Setsuhara Y 2017 Control of reactive oxygen and nitrogen species production in liquid by nonthermal plasma jet with controlled surrounding gas *Japan. J. Appl. Phys.* **56** 01AC06
- [33] Kurake N et al 2017 Effects of •OH and •NO radicals in the aqueous phase on H<sub>2</sub>O<sub>2</sub> and generated in plasma-activated medium *J. Phys. D: Appl. Phys.* **50** 155202
- [34] Kurita H, Miyamoto J, Miyachika S, Uchihashi Y, Yasuda H, Takashima K and Mizuno A 2017 Production of reactive oxygen and nitrogen species in a cell culture medium exposed to an atmospheric pressure plasma jet *MRS Adv.* **2** 987–93
- [35] Julák J, Hujacová A, Scholtz V, Khun J and Holada K 2018 Contribution to the chemistry of plasma-activated water *Plasma Phys. Rep.* **44** 125–36
- [36] Nani L, Tampieri F, Ceriani E, Marotta E and Paradisi C 2018 ROS production and removal of the herbicide metolachlor by air non-thermal plasma produced by DBD, DC<sup>-</sup> and DC<sup>+</sup> discharges implemented within the same reactor *J. Phys. D: Appl. Phys.* **51** 274002
- [37] Tarabová B, Lukeš P, Janda M, Hensel K, Šikurová L and Machala Z 2018 Specificity of detection methods of nitrites and ozone in aqueous solutions activated by air plasma *Plasma Process. Polym.* **15** e1800030
- [38] Oh J-S, Szili E J, Ogawa K, Short R D, Ito M, Furuta H and Hatta A 2018 UV-vis spectroscopy study of plasma-activated water: dependence of the chemical composition on plasma exposure time and treatment distance *Japan. J. Appl. Phys.* **57** 0102B9
- [39] Jablonowski H, Hänsch M A C, Dünnbier M, Wende K, Hammer M U, Weltmann K-D, Reuter S and von Woedtke T 2015 Plasma jet's shielding gas impact on bacterial inactivation *Biointerphases* **10** 029506
- [40] Girard F et al 2018 Correlations between gaseous and liquid phase chemistries induced by cold atmospheric plasmas in a physiological buffer *Phys. Chem. Chem. Phys.* **20** 9198–210
- [41] Janda M, Martišovits V, Hensel K and Machala Z 2016 Generation of antimicrobial NO<sub>x</sub> by atmospheric air transient spark discharge *Plasma Chem. Plasma Process.* **36** 767–81
- [42] Pawlat J, Hayashi N and Yamabe C 2001 Studies on electrical discharge effects in a foaming environment *Japan. J. Appl. Phys.* **40** 7061–6
- [43] Wandell R J, Wang H, Tachibana K, Makled B and Locke B R 2018 Nanosecond pulsed plasma discharge over a flowing

- water film: characterization of hydrodynamics, electrical, and plasma properties and their effect on hydrogen peroxide generation *Plasma Process. Polym.* **15** e1800008
- [44] Malik M A 2010 Water purification by plasmas: which reactors are most energy efficient? *Plasma Chem. Plasma Process.* **30** 21–31
- [45] Locke B R and Shih K-Y 2011 Review of the methods to form hydrogen peroxide in electrical discharge plasma with liquid water *Plasma Sources Sci. Technol.* **20** 034006
- [46] Sander R 2015 Compilation of Henry's law constants (version 4.0) for water as solvent *Atmos. Chem. Phys.* **15** 4399–981
- [47] Kruszelnicki J, Lietz A M and Kushner M J 2017 Interaction between atmospheric pressure plasmas and liquid micro-droplets *Conf. Program and Book of Abstracts, International Conf. on Plasmas with Liquids (ICPL 2017)* ed P Lukeš and K Koláček (Prague (Czech Republic): Institute of Plasma Physics CAS) p 37
- [48] Janda M, Martišoviš V and Machala Z 2011 Transient spark: a dc-driven repetitively pulsed discharge and its control by electric circuit parameters *Plasma Sources Sci. Technol.* **20** 035015
- [49] Janda M, Machala Z, Niklová A and Martišoviš V 2012 The streamer-to-spark transition in a transient spark: a dc-driven nanosecond-pulsed discharge in atmospheric air *Plasma Sources Sci. Technol.* **21** 045006
- [50] Janda M, Viktor M, Hensel K, Dvonč L and Machala Z 2014 Measurement of the electron density in transient spark discharge *Plasma Sources Sci. Technol.* **23** 065016
- [51] Machala Z, Janda M, Hensel K, Jedlovský I, Leštinská L, Foltin V, Martišoviš V and Morvová M 2007 Emission spectroscopy of atmospheric pressure plasmas for biomedical and environmental applications *J. Mol. Spectrosc.* **243** 194–201
- [52] Pongráč B, Kim H H, Janda M, Martišoviš V and Machala Z 2014 Fast imaging of intermittent electro-spraying of water with positive corona discharge *J. Phys. D: Appl. Phys.* **47** 315202
- [53] Machala Z, Jedlovský I and Martišoviš V 2008 DC discharges in atmospheric air and their transitions *IEEE Trans. Plasma Sci.* **36** 918–9
- [54] Smith M A H, Devi V M, Benner D C and Rinsland C P 2001 Absolute intensities of  $^{16}\text{O}_3$  lines in the 9–11  $\mu\text{m}$  region *J. Geophys. Res.* **106** 9909–21
- [55] Eisenberg G M 1943 Colorimetric determination of hydrogen peroxide *Ind. Eng. Chem. Anal. Ed.* **15** 327–8
- [56] Bader H and Hoigné J 1981 Determination of ozone in water by the indigo method *Water Res.* **15** 449–56
- [57] Rusterholtz D L, Lacoste D A, Stancu G D, Pai D Z and Laux C O 2013 Ultrafast heating and oxygen dissociation in atmospheric pressure air by nanosecond repetitively pulsed discharges *J. Phys. D: Appl. Phys.* **46** 464010
- [58] Van Gaens W and Bogaerts A 2014 Reaction pathways of biomedically active species in an Ar plasma jet *Plasma Sources Sci. Technol.* **23** 035015
- [59] Douat C, Hübner S, Engeln R and Benedikt J 2016 Production of nitric/nitrous oxide by an atmospheric pressure plasma jet *Plasma Sources Sci. Technol.* **25** 025027
- [60] Lowke J J and Morrow R 1995 Theoretical analysis of removal of oxides of sulphur and nitrogen in pulsed operation of electrostatic precipitators *IEEE Trans. Plasma Sci.* **23** 661–71
- [61] Pekárek S 2017 Experimental study of nitrogen oxides and ozone generation by corona-like dielectric barrier discharge with airflow in a magnetic field *Plasma Chem. Plasma Process.* **37** 1313–30
- [62] Lukes P, Locke B R and Brisset J-L 2012 Aqueous-phase chemistry of electrical discharge plasma in water and in gas-liquid environments *Plasma Chemistry and Catalysis in Gases and Liquids* ed V I Parvulescu et al (Weinheim: Wiley) ch 6
- [63] Lukeš P, Tresp H, Reuter S, Dolezalova E, Clupek M and von Woedtke T 2014 Kinetic analysis of peroxy-nitrite formation in liquids treated by air plasma *14th Int. Symp. on High Pressure Low Temperature Plasma Chemistry HAKONE 2014* ed R Brandenburg and L Stollenwerk (Zinnowitz (Germany): INP Greifswald, IfP Greifswald)
- [64] Hoigné J, Bader H, Haag W R and Staehelin J 1985 Rate constants of reactions of ozone with organic and inorganic compounds in water-III. Inorganic compounds and radicals *Water Res.* **19** 993–1004
- [65] Hefny M M, Pattyn C, Lukes P and Benedikt J 2016 Atmospheric plasma generates oxygen atoms as oxidizing species in aqueous solutions *J. Phys. D: Appl. Phys.* **49** 404002
- [66] Benedikt J, Mokhtar Hefny M, Shaw A, Buckley B R, Iza F, Schäkermann S and Bandow J E 2018 The fate of plasma-generated oxygen atoms in aqueous solutions: non-equilibrium atmospheric pressure plasmas as an efficient source of atomic O(aq) *Phys. Chem. Chem. Phys.* **20** 12037–42
- [67] Ikawa S, Tani A, Nakashima Y and Kitano K 2016 Physicochemical properties of bactericidal plasma-treated water *J. Phys. D: Appl. Phys.* **49** 425401
- [68] Goldstein S, Lind J and Merényi G 2005 Chemistry of peroxy-nitrites as compared to peroxy-nitrates *Chem. Rev.* **105** 2457–70